UNIVERSITÀ DEGLI STUDI DI PADOVA

Department of Physics and Astronomy
MSc Physics

Final Dissertation

Detection Prospects for Axion-Like Particles (ALPs) Searches with Southern Wide-Field Gamma-ray Observatory (SWGO)

Supervisor:
Michele Doro

Co-supervisor:
Ivana Batkovic

Candidate:
Muhammad Muneeb Bin Shoaib

ACADEMIC YEAR 2023/2024

To raise new questions, new possibilities, to regard old problems from a new angle, requires creative imagination and marks real advance in science.

Albert Einstein

Contents

EXECUTIVE SUMMARY

The thesis introduces the concept of Axion-Like Particles (ALPs) as the broader class of axions which are considered as a potential Dark Matter candidates in Beyond Standard Model Physics. Axions were proposed by R. D. Peccei and H. R. Quinn [1] as a plausible solution for the strong CP problem. For this study, we are mainly interested in the interaction between ALPs and photons that occurs in the presence of external electric or magnetic field. This phenomenon can help us in indirect search of ALPs by observing the ALP signatures in the spectrum of gamma rays emitted from distant extragalactic objects such as AGNs. This leads us to one of the aims of our study that is to compute the ALP models with different ALP mass and ALP-photon coupling and apply these models on the spectra of the blazar sources. In this way, we can study the change in the spectra of the sources at very high energies due to ALP-photon mixing. Secondly, the thesis focuses on the detection prospects of Southern Wide-Field Gamma-ray Observatory (SWGO). SWGO is a ground-based gamma ray detector which will be built in Southern Hemisphere and complement the Extensive Air Shower Arrays (EAS) such as HAWC and LHASSO. Chapter 1 provides the overview on the state of the art gamma-ray astronomy highlighting the current gamma-ray instruments and their progress in the field and consequently describing the need of next generation gamma-ray detector SWGO. As discussed above, ALP-photon mixing occurs in the presence of magnetic field, therefore, chapter 1 also provides description on the magnetic fields that are involved in the ALP-photon propagation. This includes the source/jet magnetic field, intracluster magnetic field, intergalactic magnetic field and finally the Milky Way galactic magnetic field.

Chapter 2 provides a detailed explanation on the selection of the blazar sources and modelling their multiwavelength spectra with online platforms such as AGNPY and MMDC. Chapter 2 also highlights the problems that we faced with the multiwavelength data of the sources and their modelling. We performed the analysis on twelve blazar sources (most intense ones) with known redshift selected from the 3FHL Fermi catalog. For the ALP analysis, we used `GammaALPs`, a python code developed to calculate ALP-photon mixing probability in various astrophysical environments and magnetic fields. Finally, chapter 3 provides all the simulation plots and results that we obtained in our study. Our results suggest that if ALPs exist and the ALP-photon mixing occurs then among the selected blazar sources, the two ALP models with ALP mass 1 neV and 10 neV are mostly affecting the spectra resulting in the excess flux values. Sources that are very far (high redshift) are detected by SWGO only if ALP-photon mixing occurs consequently making the spectra sensitive to SWGO. Few close sources are detectable with SWGO even without the the effect of ALP-photon mixing as their observed spectra lies above the SWGO sensitivity. Some sources are not detectable by SWGO as their flux is steeply falling and even if ALPs exist, their effects become observable below SWGO sensitivity. At the end, we also performed the simulation for a few sources to explore the ALP parameter space m_a = 1neV - 1μeV and $g_{a\gamma} = 1 \times 10^{-11} - 1 \times 10^{-10}$ GeV^{-1}. We derived constraints on the detectablity of the sources highlighting the parameter space that can be used to exclude ALP models in future.

Chapter 1
Introduction

Very high energy gamma-ray astrophysics is known to provide one of the possible ways to understand the origin of cosmic rays and the dynamics of their production. It is known that the detection of VHE gamma rays is very challenging due to steeply falling fluxes of astrophysical spectra and the absorption of photons in extragalactic background light (EBL) which pervade the Universe. This attenuation due to EBL is dominant at higher energies (above ~ 300 GeV). In the presence of ambient magnetic fields, gamma rays can be converted to hypothetical Axion-Like Particles (ALPs) through energy dependent oscillations. ALPs can travel through regions which are opaque to gamma rays due to the presence of background photon fields [2]. As a result of ALP-photon mixing, excess in gamma ray flux can be observed in the spectrum at very high energies that can be detected with future instruments such as CTA and SWGO [3].

1.1 Axion and Axion-Like Particles

Axion is a fundamental particle that was introduced in 1970s by R. D. Peccei and H. R. Quinn [1] as a plausible solution for the non observed violation of CP symmetry in strong interactions. The Lagrangian describing the theory of strong interactions or Quantum Chromodynamics (QCD) can be written as:

$$\mathscr{L}_{QCD} = -\frac{1}{4} G_{\mu\nu} G^{\mu\nu} + \bar{q} i \not{D} q - [\bar{q}_R m_q q_L + \text{h.c.}] \tag{1.1}$$

where $G_{\mu\nu}$ is a gauge invariant gluon field strength tensor, q is the quark field, $\not{D}$ is the gauge covariant derivative which couples the quarks with the gluon fields, in case of QCD it is given by $\not{D}_\mu = \gamma_\mu(\partial_\mu - igTA_\mu)$ where A_μ are the gluon fields and T represents SU(3) generators. The above Lagrangian is CPT invariant but there is an additional operator consistent with QCD gauge symmetry which also contributes in non-abelian gauge theories; it can be written as:

$$\mathscr{L}_{QCD} = \theta_{QCD} \frac{g^2}{32\pi^2} G^a_{\mu\nu} \tilde{G}^{\mu\nu}_a \tag{1.2}$$

where θ_{QCD} is a phase parameter, g^2 is the QCD coupling, a represents the trace summation over SU(3) colors. In case of no CP violation θ_{QCD} would be 0.

The PQ mechanism introduces a new chiral $U_{pq}(1)$ symmetry that undergoes spontaneous breaking at a high energy scale f_a. Axions are produced due to this spontaneous symmetry breaking that is introduced to preserve the CP symmetry in strong interactions. Axions can be identified as Nambu-Goldstone bosons associated with $U(1)_{PQ}$ [4]. Since their proposal, axions have been extensively studied both theoretically and observationally. In the PQ formalism, the axion is characterized by its mass m_a, which is linked to the coupling f_a and since it is a massive new particle, it can be the potential candidate for Dark Matter (DM) in Beyond Standard Model (BSM). In the original model proposed by Peccei and Quinn [1], Weinberg [4], and Wilczek [5], the axion's decay constant is approximately at the electroweak scale (around 246 GeV), with the axion's mass being inversely proportional to it. Consequently, its mass was initially anticipated to be relatively large, around the order of 100 keV.

$$m_a \simeq \frac{m_\pi f_\pi}{f_a} \simeq 0.62 \left(\frac{10^7 \text{GeV}}{f_a} \right) \text{eV} \tag{1.3}$$

where $m_\pi \simeq 135$ MeV and $f_\pi \simeq 92$ MeV. For the coupling constant f_a, two criteria must be met: the couplings should not be ruled out by experimental searches (imposing a lower limit on f), and Axion (DM) must be successfully produced in the early universe. Therefore, typical values for f_a must be close to Grand Unification Scale that is 10^{15} GeV, anticipating that axion can be as light as $m_a \simeq 10^{-9}$eV.

The Peccei-Quinn axion possesses a crucial characteristic wherein its mass and interaction strength are inversely correlated and are linked to the observed properties of pions. However, the class of hypothetical axions can be extended to a broader category of particles where their coupling is no longer coupled with mass. These entities are referred to as axion-like particles (ALPs). One phenomenological aspect of the hypothetical axion is its two-photon vertex, enabling the conversion of axions into photons in the presence of external electric or magnetic fields [6] via an interaction term which also allows the experimental detectability.

$$\mathscr{L}_{a\gamma} = -\frac{g_{a\gamma}}{4} F_{\mu\nu} \tilde{F}^{\mu\nu} a \;=\; g_{a\gamma} \vec{E} \cdot \vec{B} a \tag{1.4}$$

where $g_{a\gamma}$ is the photon-ALP coupling, $F_{\mu\nu}$ the strength tensor of the electromagnetic field, a is the axion field with mass m_a, $\vec{E}$ is the electric field of a photon beam, and $\vec{B}$ is the external magnetic field. Schematically, the ALP-photon coupling is shown in Fig.1.1:

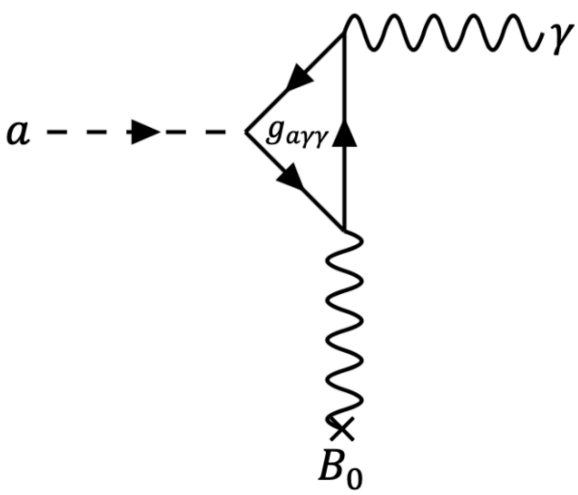

Figure 1.1: Feynamn diagram for ALP-photon coupling

1.2 ALP-Photon Mixing

The presence of axions and ALPs can be investigated through their effects on the spectra of astrophysical sources [3]. This is because ALPs interact with photons in the presence of magnetic fields. Consequently, TeV gamma rays may convert into ALPs in strong magnetic fields, traveling across cosmological distances until encountering another significant magnetic field, such as that of the Milky Way, where they may revert to observable gamma rays. These processes of conversion and reconversion are governed by a probability term for mixing $P_{\gamma\gamma}$, which is dependent on the ALP mass and coupling, as well as the characteristics of the magnetic field.

1.2.1 ALP Propagation and Probability of ALP-Photon Mixing

In order to comprehend the phenomenon of ALP propagation and their conversion and reconversion into photons in the presence of an external magnetic field, it's important to discuss the ALP-photon oscillation model. The effective Lagrangian for ALP-photon mixing can be written as:

$$\mathscr{L} = \mathscr{L}_{a\gamma} + \mathscr{L}_{\text{EH}} + \mathscr{L}_a \tag{1.5}$$

where

$$\mathscr{L}_{a\gamma} = -\frac{g_{a\gamma}}{4} F_{\mu\nu}\tilde{F}^{\mu\nu} a \tag{1.6}$$

$$\mathscr{L}_{\text{EH}} = -\frac{1}{4} F_{\mu\nu}F^{\mu\nu} + \frac{\alpha^2}{90 m_e^4}\left[(F_{\mu\nu}F^{\mu\nu})^2 + \frac{7}{4}(F_{\mu\nu}\tilde{F}^{\mu\nu})^2\right] \tag{1.7}$$

$$\mathscr{L}_a = \frac{1}{2}(\partial_\mu a \partial^\mu a - m_a^2 a^2) \tag{1.8}$$

Eq 1.6 represents the interaction term between photons and axions. Eq 1.7 is the effective Euler-Heisenberg Lagrangian accounting for corrections of QED loops in photon propagators induced by an external magnetic field [7], while Eq 1.8 models the kinetic and mass term of axion field.

ALPs exclusively interact with photons in a presence of a magnetic field component $\mathbf{B}_\perp$ perpendicular to the propagation direction $\mathbf{k}$, and solely with photon polarization states lying in the plane spanned by $\mathbf{B}$ and $\mathbf{k}$ [8]. If you consider A_1 and A_2 as the polarization states along x_1 and x_2 respectively, x_3 be the propagation direction and magnetic field component $\mathbf{B}_\perp = B\hat{\mathbf{e}}_2$, then the equations of motion for a polarized photon beam with energy E propagating in a cold plasma filled with an uniform magnetic field can be expressed in Schrödinger-like form:

$$\left(i\frac{d}{dx_3} + E + \mathscr{M}_o\right)\Psi(x_3) = 0 \tag{1.9}$$

The wavefunction $\Psi(x_3)$ can be defined as:

$$\Psi(x_3) = \begin{pmatrix} A_1(x_3) \\ A_2(x_3) \\ a(x_3) \end{pmatrix} \tag{1.10}$$

where $a(x_3)$ is the axion field strength.

In Eq. 1.9, $\mathscr{M}_o$ is the ALP-mixing matrix and can be defined as:

$$\mathscr{M}_o = \begin{pmatrix} \Delta_\perp & 0 & 0 \\ 0 & \Delta_\parallel & \Delta_{a\gamma} \\ 0 & \Delta_{a\gamma} & \Delta_a \end{pmatrix} \tag{1.11}$$

The matrix terms $\Delta_\perp$ and $\Delta_\parallel$ arise due to the effect of propagation of photons in a plasma condition and QED vacuum birefringence effect. These terms can be defined as [9]:

$$\begin{aligned} \Delta_\perp &= \Delta_{\rm pl} + 2\Delta_{\rm QED} \\ \Delta_\parallel &= \Delta_{\rm pl} + \frac{7}{2}\Delta_{\rm QED}. \end{aligned} \tag{1.12}$$

The plasma condition depends on the electron density n through plasma frequency $\omega_{\rm pl}$ which can be defined as:

$$\omega_{\rm pl} \approx 0.037\sqrt{n}\ {\rm neV} \tag{1.13}$$

The plasma effects and QED vacuum polarization can then be defined as [9]:

$$\begin{aligned} \Delta_{\rm pl} &= -\frac{\omega_{\rm pl}^2}{2E} \\ \Delta_{QED} &= \frac{\alpha E B_\perp^2}{45\pi B_{\rm CR}^2} \end{aligned} \tag{1.14}$$

where α is the fine structure constant and the critical magnetic field is $B_{\rm CR} = m_e^2/|e| \approx 4.4 \times 10^{13}$G.

The term Δ_a in Eq. 1.11 represents the kinetic term for ALP and the off-diagonal term $\Delta_{a\gamma}$ accounts for ALP-photon mixing and depends on the interaction strength $g_{a\gamma}$ and magnetic field component $B_\perp$.

$$\begin{aligned} \Delta_a &= -\frac{m_a^2}{2E} \\ \Delta_{a\gamma} &= \frac{g_{a\gamma} B_\perp}{2} \end{aligned} \tag{1.15}$$

In the simplest scenario involving a large-scale uniform magnetic field, the probability of a photon converting into an ALP or the ALP converting back to photon after traversing a distance d can be defined as [10]:

$$P_{\gamma\to a} = \frac{2\Delta_{a\gamma}^2}{\Delta_{osc}^2}\sin^2\left(\frac{d\Delta_{osc}}{2}\right) \tag{1.16}$$

where Δ_{osc} is the oscillation wave-number which appears in the probability due to the loss of photons during the conversion process and this results as an additional imaginary contribution in terms $\Delta_{\perp}$ and $\Delta_{||}$ and scaling with the mean free path of the photon. Δ_{osc} can mathematically be defined as:

$$\Delta_{osc} = \sqrt{(\Delta_a - \Delta_{pl})^2 + 4\Delta_{a\gamma}^2} \tag{1.17}$$

The ALP-photon conversion probability becomes maximum and independent of energy in the strong mixing regime (SMR) between the range $E_{crit} < E < E_{max}$ [11].

$$E_{\rm crit} \simeq 2.5 \mathrm{GeV} \frac{m_{a,\rm neV}^2 - \omega_{pl,\rm neV}^2}{g_{11} B_{\mu G}} \tag{1.18}$$

$$E_{\rm max} \simeq 2.12 \times 10^6 \mathrm{GeV} \frac{g_{11}}{B_{\mu G}} \tag{1.19}$$

where $B_{\mu G}$ is the magnetic field in micro-Gauss and $g_{11} = g_{a\gamma}/10^{-11}\mathrm{GeV}^{-1}$. The oscillation wave-number Δ_{osc} can also be written in terms of $E_{\rm crit}$ as following [9]:

$$\Delta_{osc} = 2\Delta_{a\gamma} \sqrt{1 + \left(\frac{E_{crit}}{E}\right)^2} \tag{1.20}$$

Hence the ALP-photon conversion probability can be re-written as:

$$P_{\gamma \to a} = \frac{2\Delta_{a\gamma}^2}{\Delta_{osc}^2} \sin^2 \left[\frac{g_{a\gamma} B d}{2} \sqrt{1 + \left(\frac{E_{crit}}{E}\right)^2} \right] \tag{1.21}$$

Since we cannot expect a simple hypothesis with only one magnetic field domain, the complete structure of magnetic field with multiple orientations should be accounted here but a more common approach can be to divide it into N domains and consequently the total photon survival probability $P_{\gamma\gamma}$ can be defined as [12]:

$$P_{\gamma\gamma} = \frac{1}{3} \left[1 - \exp\left(-\frac{3}{2} N P_{\gamma \to a} \right) \right] \tag{1.22}$$

1.3 Astrophysical Sources and Magnetic Fields

The extragalactic sources that emit particles at highest energies and can be observed from Earth include Active Galactic Nuclei (AGN). AGNs are supermassive black holes approximately of $\sim 10^6 - 10^{10}$ solar masses [13] and reside in center of galaxies. Our galaxy, the Milky-way also hosts a massive black hole at its center. AGNs are studied for several decades because they possess crucial characteristics. They are known for strong emission in the multiwavelength spectrum (from radio to gamma) and form an accretion disk of matter particles around the center of BH. The type of AGNs depends upon the orientation of emitted jet relative to the line of sight (LOS) of the observer. If the LOS of the observer is aligned with the jet axis, then this type of AGN is called Blazar [13]. Fig. 1.2

shows the schematic of different types of emission from AGN.

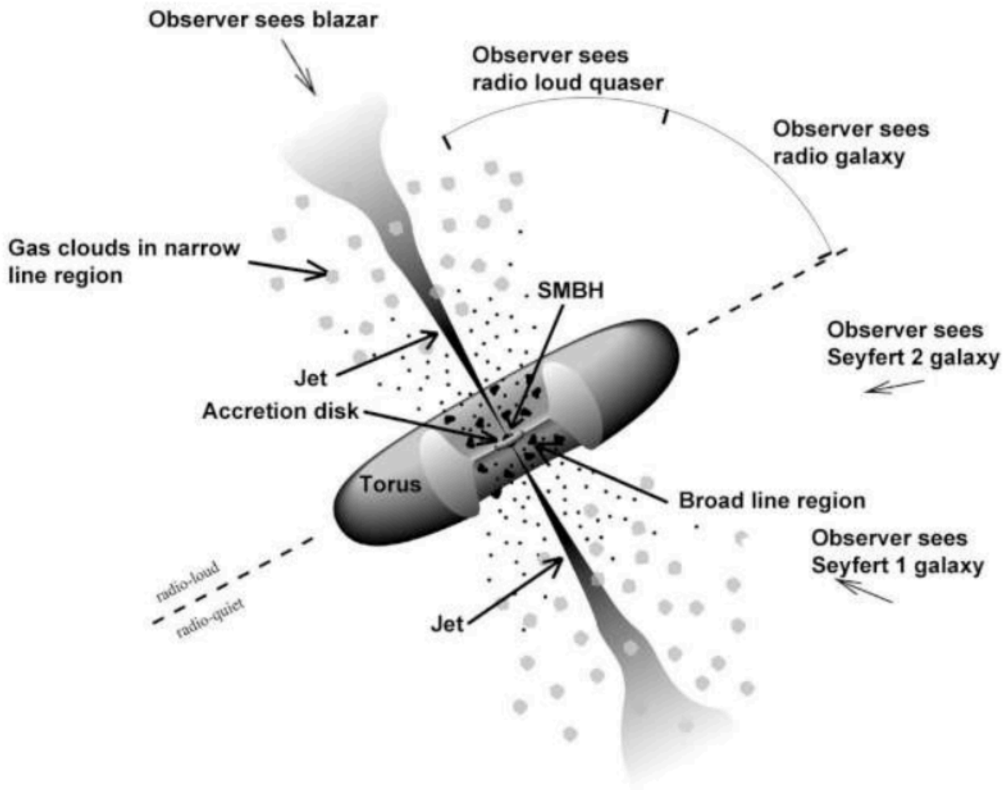

Figure 1.2: Schematic of AGN Emission [13]

In high energy astrophysics, blazars are of great interest to study as they accelerate particles to the highest observed energies. Blazars are further divided into two subclasses namely BL Lacertae objects (BL Lacs) and Flat-Spectrum Radio Quasars (FSRQs). Observational properties of both types of blazars are similar but they differ in emission lines. FSRQs have broad emission lines while BLLs have weak emission lines. In our analysis, we are interested in BL Lacs because they are dominated at high energies as they have harder spectra due to the shift in the synchrotron peak.

As the interaction between photons and ALPs solely occurs in the presence of an external magnetic field, the magnetic field environment between the photon source and the detector is crucial for predicting the expected gamma-ray spectrum on Earth. This encompasses both the magnetic fields emanating from the blazar jet itself and those from the surrounding intra-cluster magnetic field, particularly pertinent for sources situated near the core of vast galaxy clusters. This section provides a concise overview of the magnetic field models that are important for this study including the magnetic fields of the blazar jet, the intracluster magnetic field, and the Milky Way magnetic field. It's noteworthy that the source magnetic field depends on the blazar properties [14].

1.3.1 BL Lac Jet Magnetic Fields

Magnetic fields within blazar jets have been inferred through measurements across various scales, spanning from ultra-compact regions situated approximately 0.1 pc away from the central black hole to structures extending up to 100 kpc, such as lobes, plumes, and hot spots [15]. Radio observations, which track frequency-dependent positional shifts of optically thick radio cores, enable the estimation of the core's magnetic field strength, typically around 0.1 G, at a distance of 1 pc from the central black hole [16]. These values align with those deduced from modeling spectral energy distributions (SEDs) using simple synchrotron-self-compton (SSC) emission models as discussed in [17] [18], which probe the magnetic field within the very high energy (VHE) emission zone.

Active galactic nuclei (AGN) that are classified as blazars have relativistic jets directed straight towards Earth. Blandford & Konigl [19] presented the simple jet model that features a conical geometry: $R(d) = \phi d$, where R represents the radius of the jet, ϕ denotes the opening angle, and d is the distance from the base of the jet. Due to the jet's orientation towards Earth, the photon emission experiences a blue shift. Consequently, the photon energy in the comoving frame of the jet E', is linked to the energy in the laboratory frame E, through a Doppler factor δ_D given by:

$$\delta_D = \frac{1}{\Gamma_L(1-\beta_j\cos\theta_j)} \tag{1.23}$$

where Γ_L is the relativistic Lorentz factor, β_j is the beta factor $\sim v_j/c$ and θ_j is angle between the jet axis and the observer.

The magnetic field within the BL Lac jet can be characterized by both a poloidal component (aligned with the jet axis) and a toroidal component (perpendicular to the jet axis). The field strength of the poloidal component decreases as $B \propto r^{-2}$ and the toroidal component as $B \propto r^{-1}$ [20] [21]. Consequently, at sufficiently large distances from the central black hole, the toroidal component becomes dominant, and we can disregard the poloidal component in general. Assuming equipartition between magnetic and particle energies, electron densities typically range from approximately 100 to 1000 cm^{-3} at a distance of 1 pc from the core of the active galactic nucleus (AGN), with the electron density profile following $n_{elc} \propto r^{-2}$ [16]. Therefore, the magnetic field and electron density can be defined for AGN jets as follows:

$$B^j(r) = B^j_0\left(\frac{r}{r_{VHE}}\right)^{-1} \tag{1.24}$$

$$n^j(r) = n^j_0\left(\frac{r}{r_{VHE}}\right)^{-2} \tag{1.25}$$

1.3.2 Intra-Cluster Magnetic Fields

Besides the magnetic fields within the blazar jet, blazars situated within galaxy clusters may also encounter additional fields that promote ALP-photon mixing. The intracluster magnetic field can be modelled as a homogeneous field with Gaussian turbulence, defined as a field with a directional mean of zero and a variance of B^2 [11]. Due to Faraday rotation measurements and non-thermal (synchrotron) emission at radio frequencies, the turbulent magnetic fields exist in intracluster medium with the strength of micro-Gauss [22] [23]. The turbulence adheres to a power-law spectrum $M^k \propto k^q$ between the minimum (k_L) and maximum (k_H) turbulence scales. The magnetic field is radially dependent on electron density as follows [11]:

$$B^{ICM}(r) = B_0^{ICM} \left(\frac{n_r}{n_0}\right)^{\eta} \tag{1.26}$$

The electron density in this case can be parametrized as:

$$n^{ICM}(r) = n_0^{ICM} \left(1 + \left(\frac{r}{r_c}\right)^2\right)^{\frac{-3}{2}\beta_{ICM}} \tag{1.27}$$

where r_c represents the core radius and the electron density is usually 10^{-3}cm^{-3}.

There are other intracluster magnetic field models as well. Such as magnetic field derived in [24], as a solution to Grad-Shafranov equation. In this model, the field strength vanishes on the cavity surface while the interior is filled by a large scale magnetic field.

1.3.3 Inter-Galactic Magnetic Fields

Magnetic field that is present between the galactic mediums can also play the role in this phenomenon. According to the current studies, the limits of IGMF are $10^{-16} \leq B^{IGMF} \leq 10^{-9}$ [25] [26] [27] . Considering the energy density of this magnetic field and the energy density of the Cosmic Microwave Background (CMB), the effect of IGMF is negligible on particle attenuation [28]. One of the reasons is that the synchrotron losses of this IGMF are much less compared to the inverse compton scattering losses due to CMB. Additionally, the pair-conversion probability for particle transport over gigaparsec (Gpc) distances remains much lower than expected in the magnetic fields near blazars and within the Milky Way.

1.3.4 Milky-way Galactic Magnetic Field

The crucial part of ALP-photon conversion occurs in the presence of Milky-way magnetic field where ALPs are converted back to photons which can be detected on earth [29]. In [30], Jansson and Farrar have discussed the coherent component magnetic field model that is also used in `GammaALPs` calculations which we are using in our analysis [31]. `GammaALPs` is a python package developed for solving the equations of motion of the photon-ALP system using the transfer matrix method. It also provides code for calculation of mixing probability between ALPs and photons in various astrophysical environments and magnetic field models.

1.4 The Extragalactic Background Light (EBL)

Gamma rays emitted by a very distant blazar objects provide useful insights in theoretical and observational astrophysics. The detection of very high energy gamma rays becomes challenging due to the pervasive photon background called EBL. The EBL consists of photons emitted by the galaxies, stars and AGN over the evolution of the Universe. Throughout the lifetime of the Universe, this EBL is altered by the redshift due to the expansion of the Universe. The energy of EBL photons ranges from $\sim 10^{-3}$ eV to 10 eV [32]. This corresponds to the wavelengths from from the far-infrared to the near-ultraviolet (0.1 - 1000 μm). Direct measurement of EBL is itself difficult due to the light background from objects and galaxies in the surroundings. There are various numerical and analytical models published to calculate the EBL energy density and determine correct EBL spectrum. For instance, Fig. 1.3 shows the EBL energy density over the energy range ($\sim 10^{-3}$ eV to 10 eV) for sources present at different redshifts (distance). This is the model developed by Finke [33].

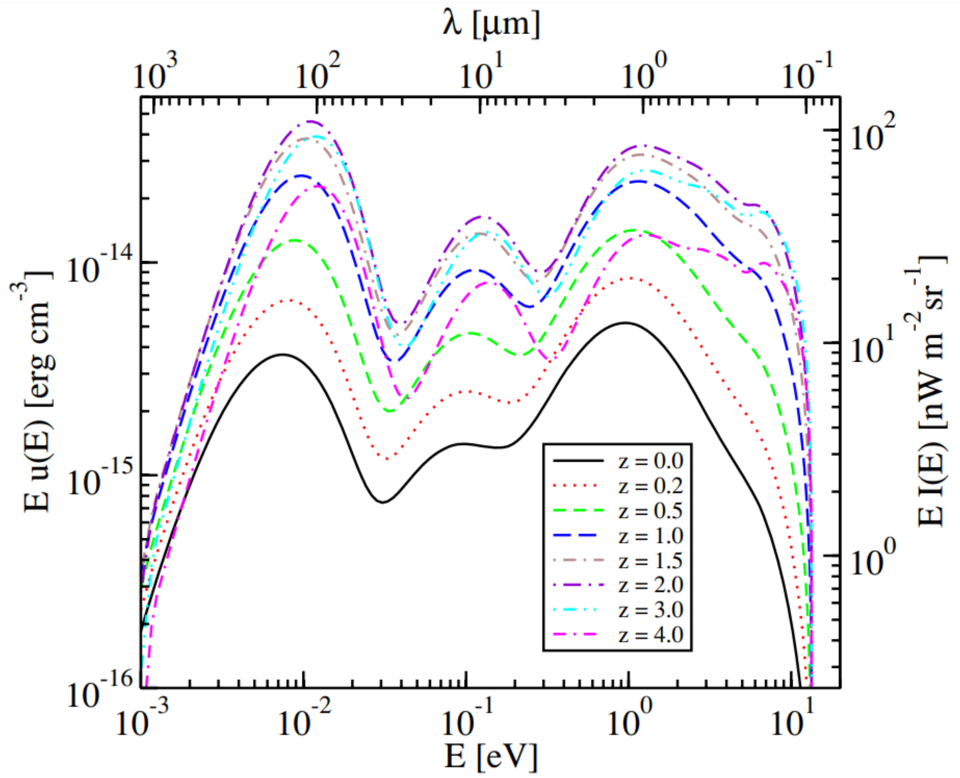

Figure 1.3: EBL energy density vs photon energy for various redshifts [33]

Due to these low energy photons present in the EBL, the interaction of high energy photons coming from a distant blazar source interact with them which leads to the pair production of electron-positron [34]. Using the particular EBL model, attenuation in the high energy photons due to the EBL can be calculated. The attenuation in the flux of gamma-ray with energy E along its path from the source at distance z can be expressed as Eq.1.28 below [32]:

$$I(E,z) = I_0 e^{-\tau(E,z)} \tag{1.28}$$

where I_0 is the flux at the source and τ is the optical depth dependent on the photon number density and cross section of the interaction of photons. It is directly proportional to the energy [32], and therefore we observe the severe EBL attenuation effect at very high energies in the multiwavelength spectra of the blazar sources. In this study, we have used the Dominguez 2011 model [35] for EBL attenuation. Fig. 1.4 shows the flux attenuation calculated in the work done by Dominguez [35].

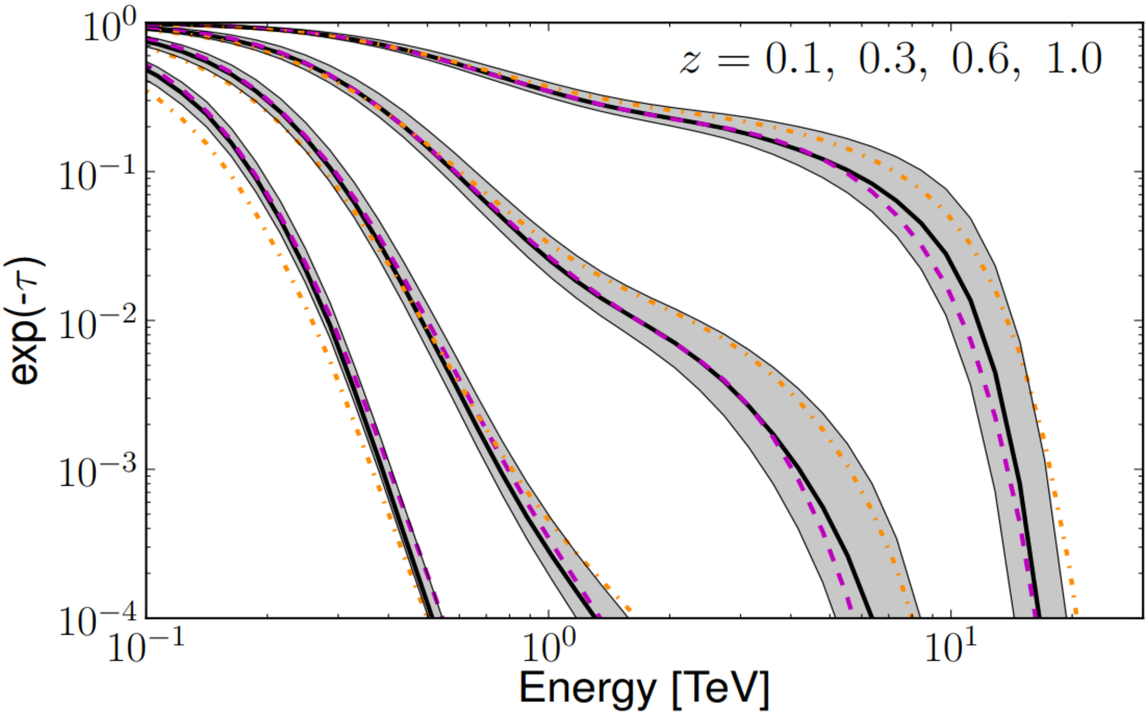

Figure 1.4: Flux attenuation vs observed gamma-ray energy calculated for various redshifts using 3 different models: Dominguez (Black), Franceschini (Purple) [36] and Gilmore (Yellow) [37]. The Grey shaded regious shows the EBL uncertainties [35].

1.5 Ground-Based Gamma-ray Astronomy

Direct detection of astrophysical gamma rays in GeV regime is only possible with space-telescopes such as Fermi-LAT, but due to the size limitations and cost feasibility, the efficiency of satellite-based detectors is always restricted. Gamma rays can also be detected indirectly especially at energies higher than Fermi-LAT (TeV range), thanks to ground based instruments. Powerful arrays of imaging atmospheric Cherenkov telescopes (IACTs) are located in both hemispheres: MAGIC (Major Atmospheric Gamma Imaging Cherenkov Telescopes) [38] and VERITAS (Very Energetic Radiation Imaging Telescope Array System) [39] in the North and HESS (High Energy Stereoscopic System) [40] in the South. However, when it comes to ground-level particle detectors, only the Northern Hemisphere is equipped with the HAWC (High Altitude Water Cherenkov Observatory) [41] and LHAASO (Large High Altitude Air Shower Observatory) [42].

IACTs have limited field of view (FOV$\sim 4^\circ$ diameter) and duty cycle ($\sim 10-15\%$) due to the need of dark and clear sky. They have angular and energy resolution of $\sim 0.1^\circ, 15\%$ and a background rejection power of $10^{-3}-10^{-2}$ with more than 70% gamma-ray efficiency [43]. The imaging technique involves detecting the Cherenkov light distribution images from electromagnetic cascades on the ground. This allows for the determination of both the longitudinal and lateral development of the electromagnetic showers, as well as the arrival direction and energy of the primary gamma rays. These detectors usually use a parabolic or spherical mirror to focus the Cherenkov photons onto a densely packed array of photomultiplier tubes (PMTs) positioned in the focal plane [44]. The detection technique of IACTs is shown in Fig.1.5.

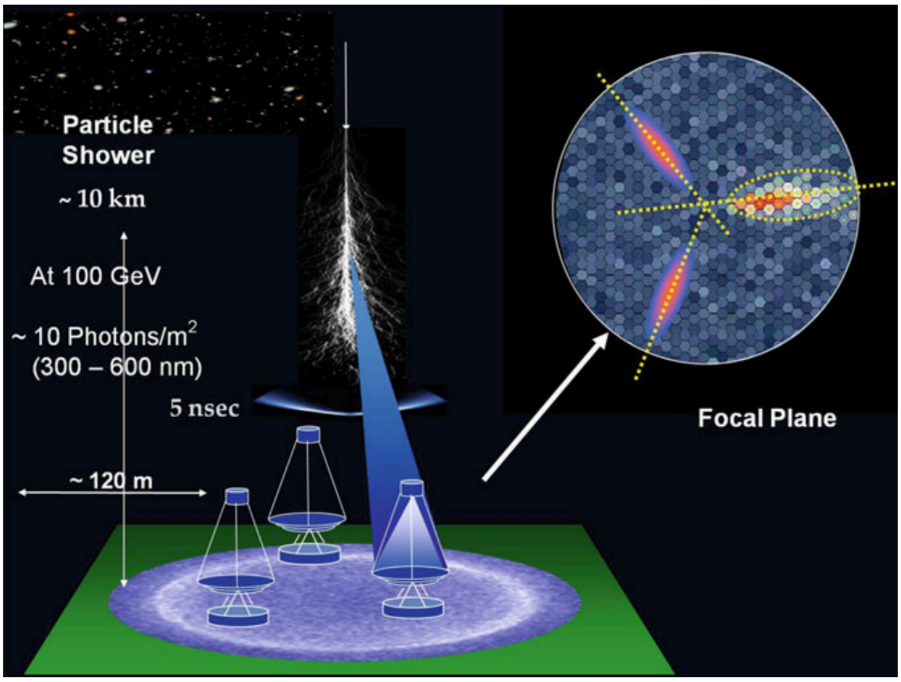

Figure 1.5: Working technique of IACTs [32]

Recently, ground-level particle detection technique is considered a good complementary approach in gamma-ray astronomy due to the limitation of duty cycle in IACTs. In the Northern hemisphere, HAWC is situated at an elevation of 4100 meters (13,500 feet) on the slopes of the Sierra Negra volcano near Puebla, Mexico. It has an instantaneous field of view that covers 15% of the sky, and over each 24-hour period, it is able to observe two-thirds of the sky [44]. HAWC consists of an array of 300 water Cherenkov detectors, each made from water storage tanks that are 5 meters high and 7.32 meters in diameter, covering an instrumented area of about 22,000 sq.meters [45]. The actual tank coverage is 12,550 sq.meters, resulting in a coverage factor of less than 60%. Fig.1.6 shows the layout of HAWC experiment.

Moreover, LHAASO is also one of the recently built ground-based particle detectors and has been successful in detecting the galactic sources in PeV range [46]. Due to its unprecedented sensitivity and capability of background rejection, LHAASO detected the large number of ultra-high energy cosmic rays in the Milky-way. LHAASO is built on Haizi Mountain, 4,410 meters above sea level, and the site covers around 1.36 square kilometers. LHAASO has also been looking for signatures of WIMPs which are potential candidates for Dark Matter. LHAASO is considered as the most sensitive gamma-ray detector in the Northern hemisphere spanning its range from few hundred GeV to PeV.

Along with these powerful detectors in the North, the installation of ground-based particle detector in the Southern hemisphere can provide great opportunity for significant scientific breakthroughs especially because of a vintage point to observe galactic center. It can help us to advance our current knowledge of gamma-ray astronomy and beyond Standard Model Physics.

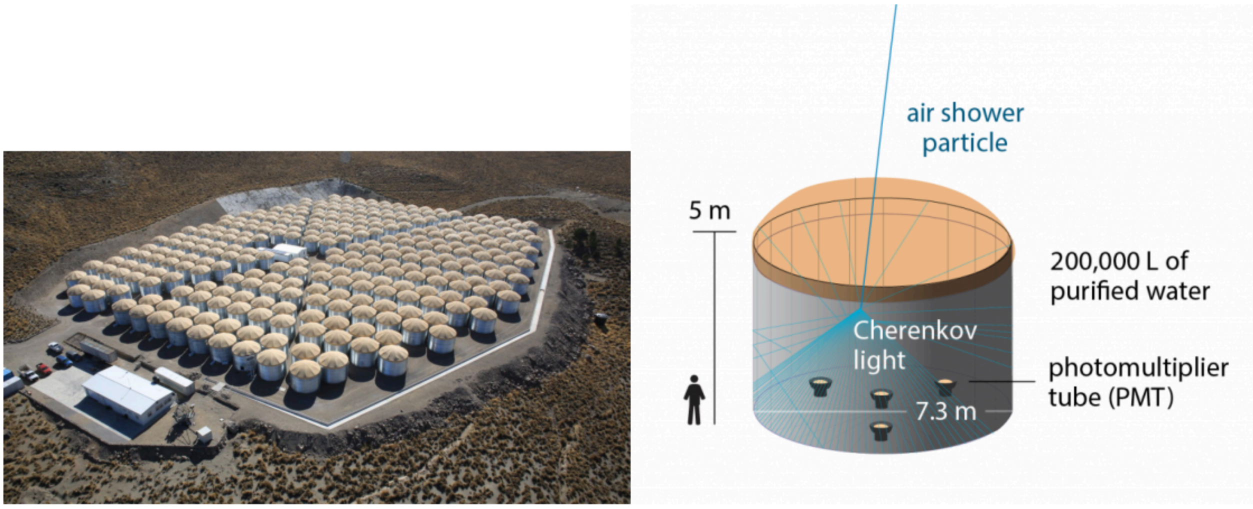

Figure 1.6: HAWC experiment (Right: Water tank used in HAWC) [44]

1.6 Next Generation Wide-Field Observatory - SWGO

SWGO (Southern Wide-filed Gamma-ray Observatory) is a next-generation ground-based gamma-ray detector which will be built in Southern Hemisphere and complement the Extensive Air Shower Arrays (EAS) such as HAWC and LHASSO [43]. It is based on water cherenkov detectors and will cover the energy range possibly from 100 GeV up to 10 PeV. It will be located in South America at a latitude between 10-30 degrees south. Fig.1.7 shows the schematic of SWGO based on water cherenkov detectors.

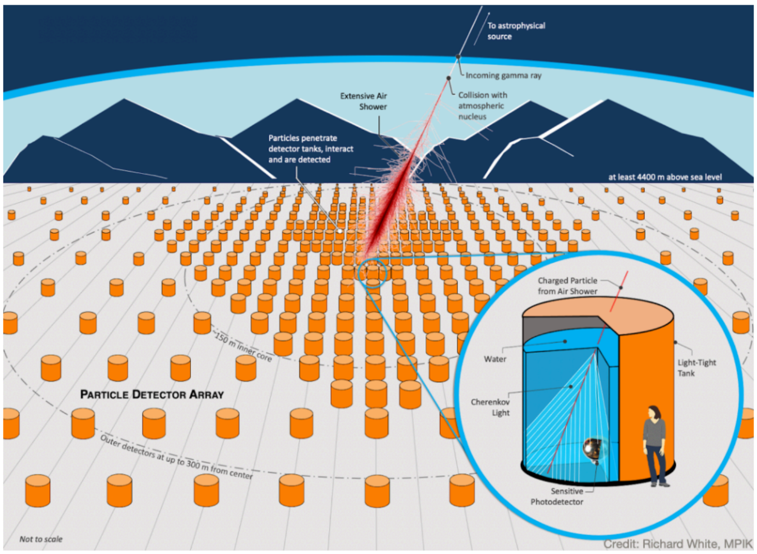

Figure 1.7: Water based cherenkov detector SWGO (`https://www.swgo.org/SWGOWiki/doku.php`)

There are many benefits of particle detection from south site such as accessing the galactic centre, Fermi bubbles, and key to local extragalactic objects. It also provides the opportunity to complement the CTAs planned studies for detecting the high mass thermal relic WIMPs annihilating in the center of galaxy [43]. Moreover, axion-like particle searches can be done where conversion of gamma-rays to ALPs can produce distinctive features in the spectra of gamma-ray sources and increase transparency of the Universe as ALPs can traverse the regions which are opaque to photons due to EBL. SWGO also aims to search for Primordial black holes with an order of magnitude bigger than the recent searches in the field. SWGO can help in triggering the CTAs and the wider community with the characterization of high flux states in AGNs and Galactic variable objects. Moreover, SWGO will be able to probe the whole range of timescales variability in the gamma-ray sky as shown in Fig. 1.8 [43] [47].

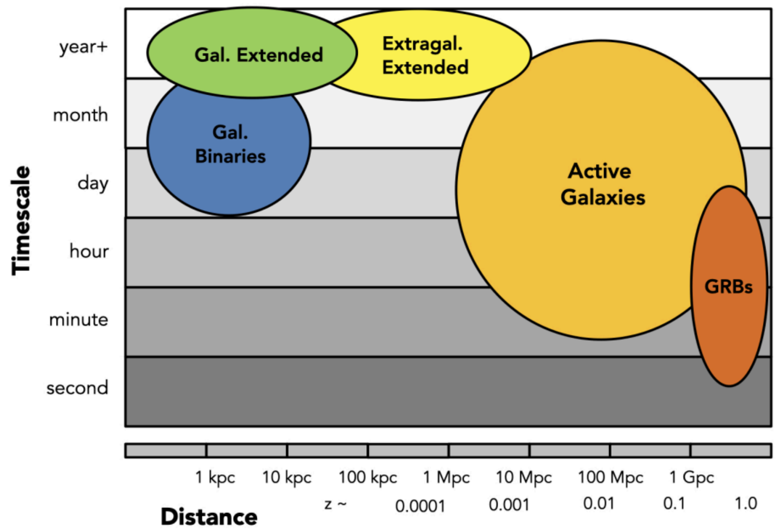

Figure 1.8: VHE transient source classes and their variability timescales [43]

1.7 Literature Review

Axions were postulated in 1977 to solve the strong CP problem in QCD. If axions have the low mass within specific range, they can be the potential candidates for cold Dark Matter. There are many experiments that have been carried out in order to search for axions. Experiments including CERN Axion Solar Telescope (CAST) [48] and International Axion Observatory (IAXO) [49] use special helioscopes to search for axions that are produced inside the sun by the conversion of plasma photons in charged particles. This process is called Primakoff process. Another type of experiment is "light-shining-through-the-wall (LSW)" experiment. In these type of experiments photons from strong laser beam are searched acrossed the wall which is possible in the case of photons converting into ALPs. This experiment is being carried out at CERN as the Optical Search for QED Vacuum Bifringence (OSQAR) [50]. The theoretical confirmation of a phenomenon in which axions can be converted into photons in a resonant cavity motivated few other modern experiments including Quest for Axions experiment (QUAX) [51] and Axion Dark Matter experiment (ADMX) [52]. These experiments are a direct search for galactic dark matter in the form of axions or ALPs and they are focused on the operation of a ferromagnetic haloscope, based on the axion-electron interaction. High energy Astrophysics searches for ALPs in the excess photon flux that can be detected on earth if the ALP-photon conversion occurs in the presence of cosmic magnetic fields [3]. The conversion is possible in magnetic fields of Active Galactic Nuclei (AGN) jets, intracluster magnetic fields, intergalactic magnetic field and in Milky-Way Galaxy.

In the past 25 years, ALP-photon conversions have been proposed as a mechanism to overcome the opacity of the extragalactic sky to high-energy radiation caused by pair production on the EBL [3]. Notably, recent observations of cosmologically distant gamma-ray sources by ground-based gamma-ray telescopes revealed unexpectedly high degree of transparency of the Universe to very high-energy (VHE) photons (greater than 100 GeV) [53] [54]. These observations suggest a lower EBL density than anticipated or significantly harder injection spectra than initially expected. The oscillation between VHE photons and ALPs could provide a feasible explanation for this phenomenon, acting as a cosmic "light-shining-through-wall" effect. Hooper and Serpico [55] were among the first who predicted that ALPs can be detected with gamma-ray telescopes. They also also predicted that IACTs such as MAGIC, VERITAS, and H.E.S.S., could have probed the range of axion mass $(10^{-9} - 10^{-3})$ eV with sensitivities stronger than CAST as can be compared from Fig.1.9 and Fig.1.10. In 2007, De Angelis [56] presented the idea of photons mixing with light spin-zero bosons (ALPs) to overcome the EBL effects in the observed photon spectra and predicted that this phenomenon can be observed with the gamma-ray telescopes. One of the first studies on searches of ALPs in gamma-ray flux is done by Sánchez-Conde [57] in which they studied the ALP-photon conversion framework for the first time simultaneously taking place in the gamma-ray source and in the intergalactic magnetic fields. The study focused on the sources 3C 279 and PKS 2155-304. In 2009, Mirizzi [58] presented the work on stochastic conversions of high energy photons into ALPs in extragalactic magnetic fields. They studied the absorption of photons in the EBL in terms of photon transfer function on the Earth. Their work also investigated deviations in the photon flux when ALP-photon conversion is involved in the presence of the turbulent structure of extra-galactic magnetic fields. This kind of structure of magnetic fields induces stochastic behaviour in the statistical distribution of the photon transfer functions. Since the start of 2010s, ALP searches using the data collected by gamma-ray telescopes drew a lot of attention of astrophysics community. H.E.S.S. made one of the first attempts to constrain the ALPs with gamma-rays using the data from the BL Lac object PKS 2155-304 [59]. MAGIC also did the study on the searches of ALPs by analyzing the 41.3 hours of observational data from the Perseus Galaxy Cluster [60].

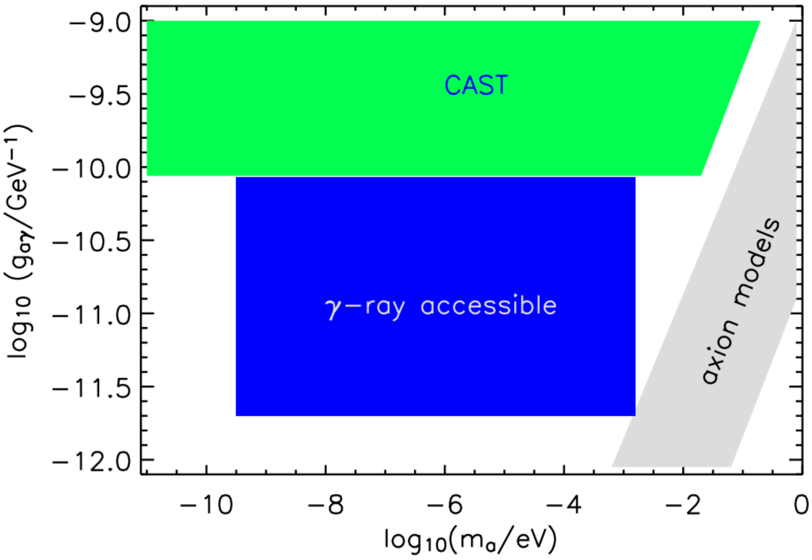

Figure 1.9: ALPs parameters range and the parameters exlcuded by CAST [55]

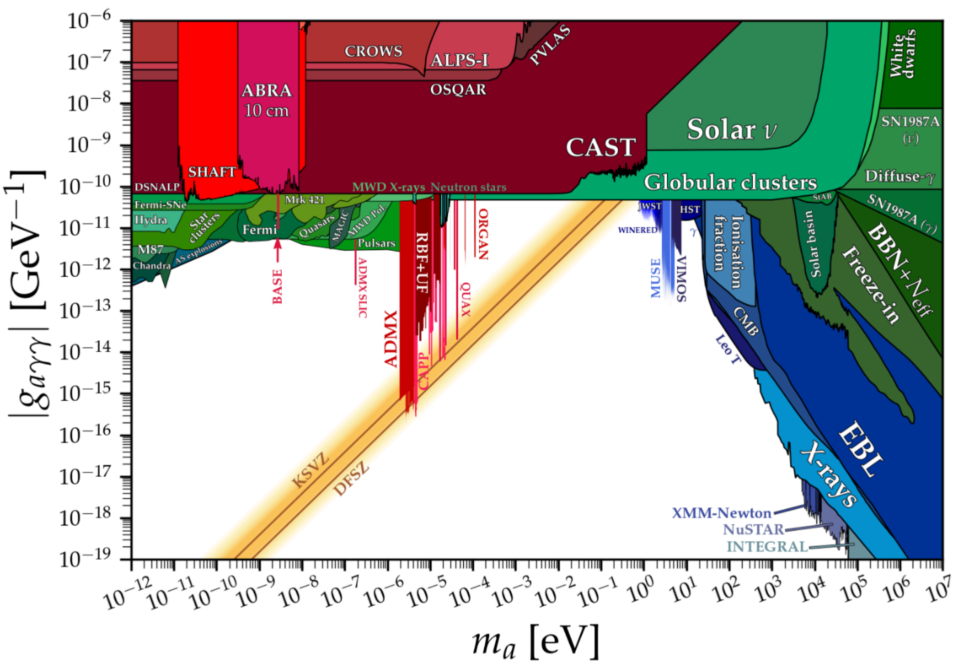

Figure 1.10: ALPs parameter space with current constraints (last update: Jan 2024). `https://cajohare.github.io/AxionLimits/`

On the other hand, ground-level particle detectors such as HAWC and LHAASO are producing results to investigate ALP effects in the observed gamma-ray spectra. In March 2022, Jacobsen [2] with her colleagues worked on constraining the Axion-Like Particles using HAWC observations of TeV Blazars. They performed the analysis for nine blazars and found that ALP coupling constant should fall below $\sim 3 \times 10^{-11}\text{GeV}^{-1}$ for ALP masses below 300 neV [2]. In their study, ALP parameters are constrained with the data from 1ES 0229, VER J0521 and PKS 1222. As for the other sources, expected flux with and without ALPs fall below the HAWC sensitivity and therefore their observations cannot be used to constrain ALPs. Fig.1.11 shows the combined constraints on ALP parameter space evaluated in their study, with the exclusion of parameter space at significance lever higher than 3σ.

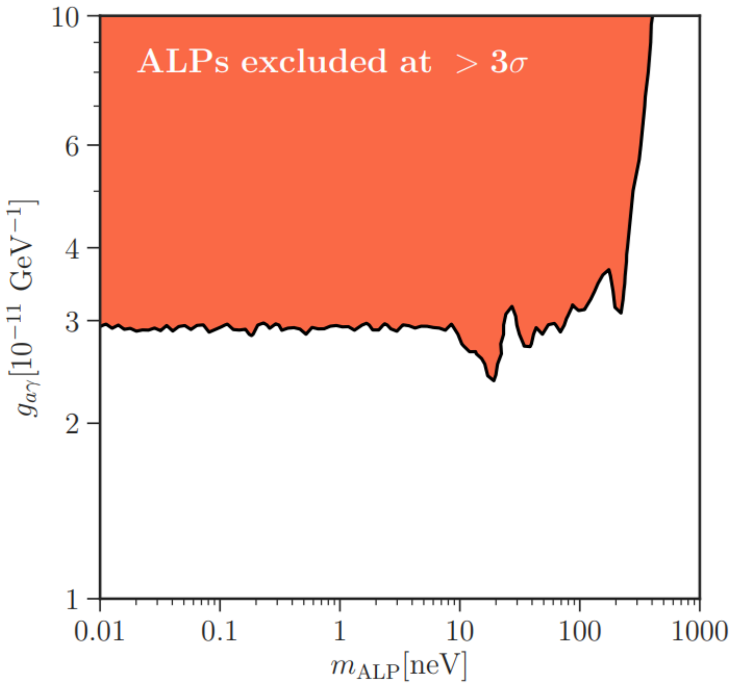

Figure 1.11: Excluded ALP parameter region at $> 3\sigma$ [2]

In June 2022, Mastrototaro [61] set the constraints on ALP parameter space using the diffuse gamma-ray flux measured by the Large High Altitude Air Shower Observatory (LHAASO). They performed the analysis in the energy range of 10 - 500 TeV using the latest data collected by LHAASO to constrain the ALP-photon coupling. The excluded values for ALP coupling strength $g_{a\gamma} > 3.9 - 7.8 \times 10^{-11}\mathrm{GeV}^{-1}$ are at 95% CL for axion mass $m_a \sim 4 \times 10^{-7}\mathrm{eV}$ [61]. Another study on exploring the ALP parameter space using the observations of galactic sources detected by LHAASO has been done in January 2024 by Li [62]. In the paper, authors investigated ALP-photon oscillation effect on the gamma-ray spectra of four galactic sources including the Crab Nebula, LHAASO J1908+0621, LHAASO J2226+6057, and LHAASO J1825-1326. The paper concludes that the ALP-photon coupling greater than $1.4 \times 10^{-10}\mathrm{GeV}^{-1}$ can be excluded for the ALP mass of $m_a \sim 4 \times 10^{-7}\mathrm{eV}$ at 95% C.L. [62]. Fig.1.12 shows the excluded parameter space for ALPs obtained in their study and it can be seen that the observations of the galactic sources by LHAASO have put more stringent constraints on the parameters as compared to the previous study done by Bi [63].

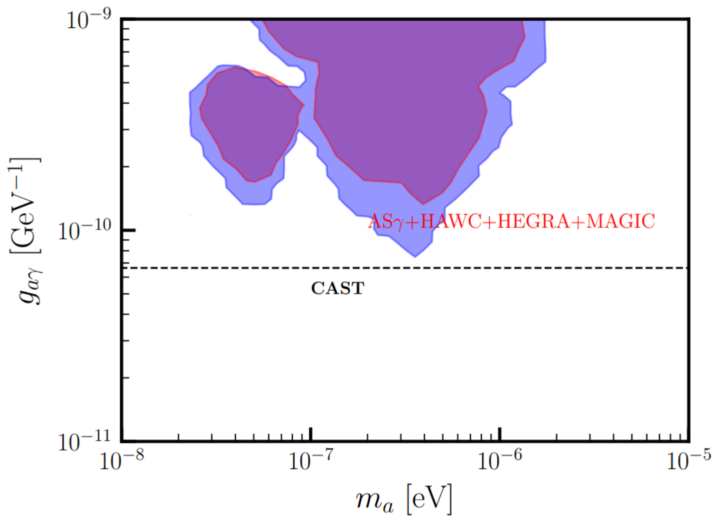

Figure 1.12: Constraints from observations of the Crab Nebula, combining the data from LHAASO and other works [62].

1.8 Problem Statement / Objective

Our work is based on the same analysis that has been done with HAWC and LHAASO as explained in the previous section. But we are studying the prospects for SWGO which is the next generation wide-field gamma-ray observatory with high duty-cycle view of the Southern sky [43]. The aim of my thesis is to test the sensitivity performance of proposed SWGO and anticipate how many GeV sources can be detected by SWGO if ALP-photon conversion occurs. This effect is expected at higher energies (even above TeV) making the SWGO experiment suitable for such study. Fig.1.13 shows the sensitivity curves for different experiments and the prospective one-year SWGO phase-space that we are also using in our analysis. The study also explores the constraints on parameter space (mass and coupling) of ALPs as shown in Fig.1.10. In this work we are focusing on ALPs masses spanning from μeV to neV and coupling strength of 1×10^{-10} GeV^{-1} and 1×10^{-11} GeV^{-1}.

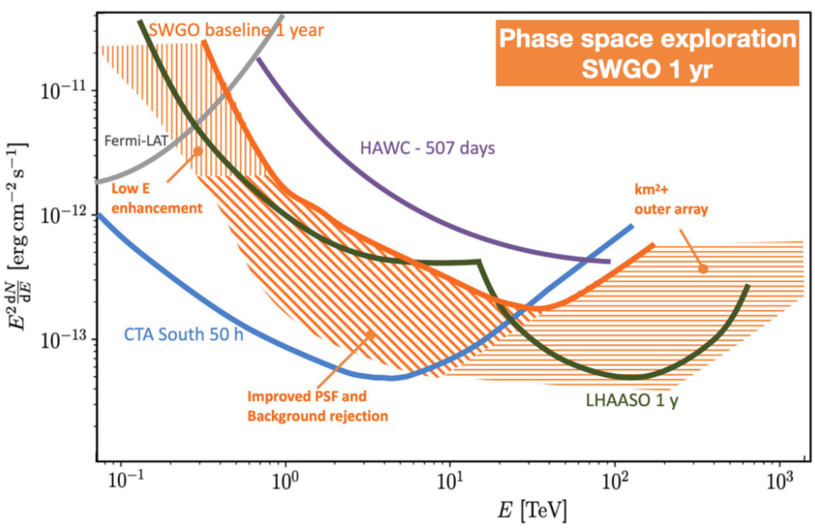

Figure 1.13: Differential point sensitivity of several experiments and 1 year phase space of SWGO [64]

Chapter 2
Methodology

This study is based on five steps. These steps will be discussed in detail in the next sections but here follows a brief description of each step.

- First step is to select the blazar sources. Among blazars, we are only interested in the hardest and the most intense BL Lac objects.
- Second step is to access the multiwavelength blazar data and prepare it for modelling. Cleaning the data is an important task because the data that we are working with contains upper limits, repeated catalog data and many outliers that can affect the fit results.
- Third step is to obtain the intrinsic spectral points by deconvoluting the observed points with EBL attenuation for the corresponding redshift of the source. For the EBL model, we used "Dominguez 2011" [35].
- Fourth step is the most important step, and it is to model the intrinsic SED to get the extrapolated spectra to the energies of interest for SWGO (GeV- TeV). This can be done in two ways, one is to use mathematical test functions like power law or broken power law and the other is to use physical particle radiative processes that occur inside AGN jets to build a model-based fit.
- The final step is to apply the ALP model computed using `GammaALPs` on the modelled intrinsic spectra to observe the ALP signatures in the flux at higher energies and check the detection of the source with SWGO.

2.1 Fermi-LAT and Source Catalogs

In our analysis, the blazar sources are selected from the Fermi-LAT 3FHL catalog [65]. Therefore, it is important to briefly discuss the Fermi telescope and its operation since 2008. Fermi Gamma-ray Telescope was launched to observe the gamma-ray sky and make advancements in the field of high energy astrophysics. The telescope consists of two main scientific instruments namely, the Gamma-ray Burst Monitor (GBM) and the Large Area Telescope (LAT). LAT is a pair production telescope based on silicon strip trackers and a Cesium Iodide calorimeter [66]. It also contains a plastic scintillator anticoincidence system that covers the tracker array, a programmable trigger, and data acquisition system. LAT is an imaging, wide field-of-view (FoV) telescope covering the energy range of 20 MeV to more than 500 GeV, with a FoV of about 2.4 steradians [67]. The overview of the space observatory is shown in Fig. 2.1.

LAT observes more than 20% of the sky all the time covering the entire sky every three hours. The measurements obtained from the instruments of LAT are used to determine the arrival direction, arrival time and energy of photons. LAT has been operating for more than 14 years in a good condition. It has completed more than 5000 days of science mission and 75500 orbits since its launch [67]. Table 2.1 shows some characteristics of LAT.

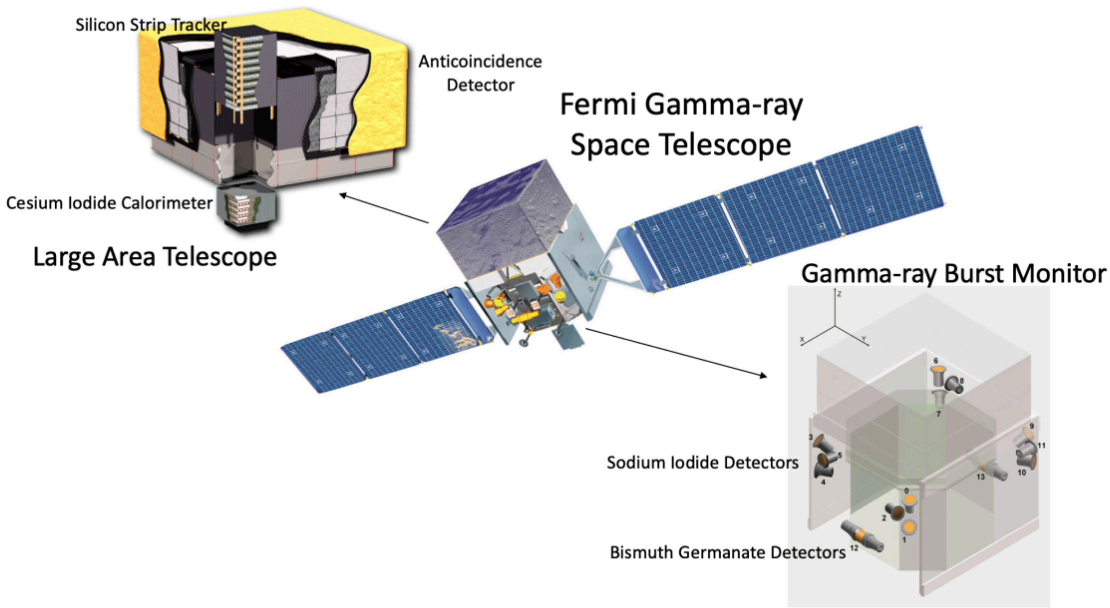

Figure 2.1: Fermi Gamma-ray Telescope with GBM and LAT [67]

Quantity	**Minimum LAT Specifications**
Energy	20 MeV - 300 GeV
Peak Effective Area	> 8000 cm^2
Field of View	> 2 sr
Angular Resolution	$< 3.5°$ (100 MeV) $< 0.15°$ ($>$ 10 GeV)
Energy Resolution	$< 10\%$
Source Location Determination	$< 0.5'$
Point Source Sensitivity	$< 6 \times 10^{-9}$ cm^{-2} s^{-1}

Table 2.1: Specifications of LAT (`https://fermi.gsfc.nasa.gov`)

The working principle of LAT can be seen in Fig. 2.2. The incoming gamma rays first pass through the anticoincidence detector which helps in distinguishing charged particles. Gamma rays continue passing through the inner conversion foil until it interacts with the tungsten foils, producing two charged particles, an electron and a positron. Finally, the charged pairs are stopped by cesium iodide calorimeter and measures the total deposited energy [66].

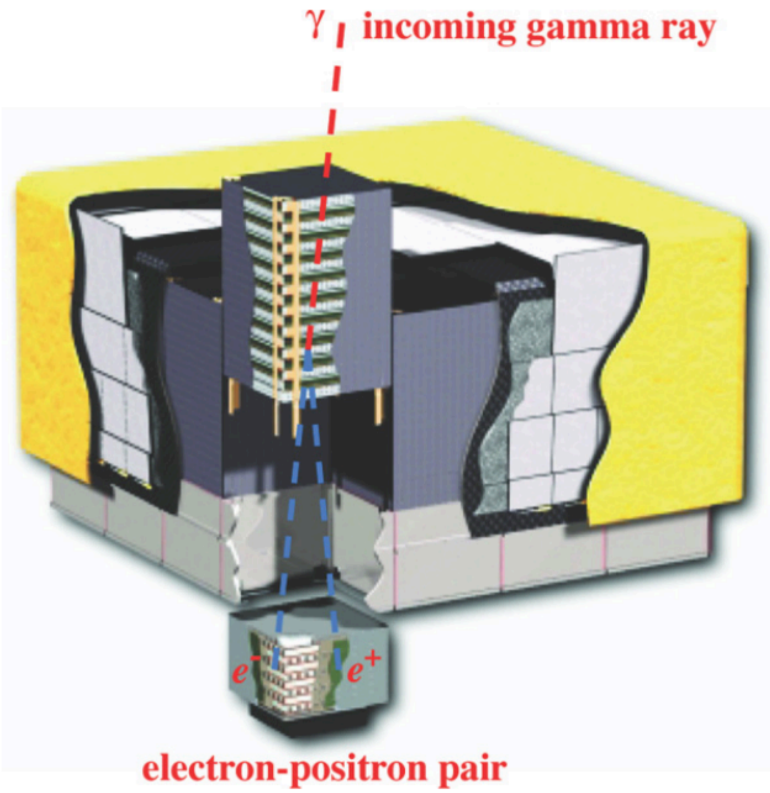

Figure 2.2: Schematic of LAT [66]

2.1.1 4FGL Catalog (DR Releases)

The fourth catalog of Fermi-LAT was released in 2020 after surveying the gamma-ray sky for eight years. It contains 5064 sources detected in the energy range of 50 MeV to 1 TeV [68]. If compare to the previous catalogs, 4FGL has a number of analysis improvements, including an updated model for the Galactic diffuse gamma-ray emission, and two sets of light curves (1-year and 2-month intervals). 4FGL catalog does not contain transient gamma-ray sources which are detectable only for short duration, including Gamma-ray bursts, solar flares, and most novae [69].

2.1.2 3FHL Catalog

The third catalog of Fermi-LAT reports hard sources at energies above 10 GeV. The catalog is published after 7 years of data collection by LAT. The catalog provides various characteristics of sources including energy flux, flux density, spectrum type, spectral index, significance, right ascension and declination. There is a total of 1556 sources available in the 3FHL catalog with 1231 extragalactic sources among which 750 are BL Lacs and 172 are FSRQs [65]. Table 2.2 shows the summary of all Fermi-LAT catalogs released up to date.

Catalog	Energy Range	Sources
1FGL	0.1 – 100 GeV	1451
2FGL	0.1 – 100 GeV	1873
3FGL	0.1 – 300 GeV	3033
FGES	10 GeV – 2 TeV	46
3FHL	10 GeV – 2 TeV	1556
FHES	1 GeV – 1 TeV	24
4FGL	50 MeV – 1 TeV	5064
4FGL-DR3	50 MeV – 1 TeV	6658
4FGL-DR4	50 MeV – 1 TeV	7194

Table 2.2: Summary of LAT Catalogs [68]

2.2 Blazar Selection

The original idea of the work was to extrapolate the complete sample of blazar sources collected by LAT in order to make strong predictions on the sensitivity performance of SWGO and also constrain ALP parameters with more authenticity. Therefore, we started to work with the Fermi-LAT 4FGL-DR3 catalog. There is a total of 6658 sources in the catalog among which only 1435 are BL Lac type blazars [70]. After modelling some of the sources using `Gammapy` spectral models, we realized that it was almost impossible to model these many blazars in this project time due to the fit failures as will be discussed in later sections. After doing analysis on few blazars sources, we, therefore decided to work with the 3FHL Fermi catalog instead of the 4FGL. 3FHL catalog contains less blazar sources as compared to 4FGL but it covers the high energy range (up to 2 TeV). We started with the hardest and the most intense blazars with the power law index ≤ 4 and flux normalization $\geq 5\times10^{-12}$ GeV^{-1}cm^{-2}s^{-1}. For our analysis, it was necessary to select the sources with known redshift as we had to extrapolate the spectra to TeV energy regime. Some of the selected blazar sources can be seen in Fig.2.3.

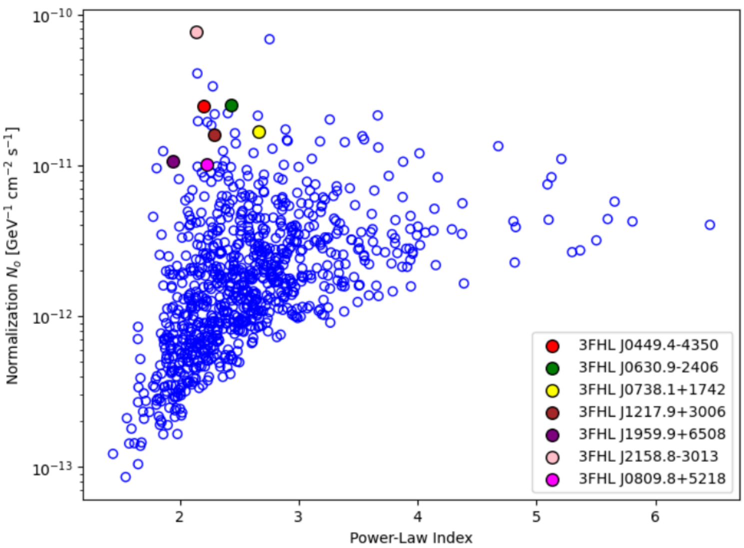

Figure 2.3: Selected (colored) sources from 3FHL Fermi Blazars [65]

We did the analysis for around thirty blazar sources in 3FHL but for some of them, the fit on the observed data was not satisfactory and therefore, we did not apply the ALP analysis on those sources. The sources that were considered for the analysis will be discussed with their spectral properties and fit results in chapter 3.

2.3 SED Modelling with Gammapy

After the selection of blazar sources, the next step was to access the blazar data and model them. We started to work with `Gammapy` [71] which is an open-source python package that serves as a core library for analysis of data from several gamma-ray instruments including IACTs and Fermi-LAT. `Gammapy` provides the library for catalog registry using which one can easily access the flux data for all Fermi-LAT catalogs. `Gammapy` provides the script for fitting the spectral points data with mathematical test functions as discussed below.

2.3.1 Spectral Models - Gammapy

The test functions were used to fit the flux data depending on the spectrum type of the sources. These functions include power law (PL), exponential cut-off power law (ECPL), exponential cut-off log-parabola (ECLP), log-parabola (LP) and broken power law (BPL). Mathematically, these functions are defined in the following Eq.[2.1 - 2.5] respectively. Some fitting parameters such as spectral index and pivot energy are chosen based on the source data given in the catalog and are added to the test function manually while performing the fit.

$$\phi(E) = \phi_o \left(\frac{E}{E_o}\right)^{\gamma} \quad (\textbf{PL}) \tag{2.1}$$

$$\phi(E) = \phi_o \left(\frac{E}{E_o}\right)^{\gamma} \exp\left(\frac{-E}{E_{cut}}\right) \quad (\textbf{ECPL}) \tag{2.2}$$

where ϕ_o is a prefactor with units ($\mathrm{cm}^{-2}\mathrm{s}^{-1}\mathrm{MeV}^{-1}$), E_o is the pivot energy, γ is the power-law index and E_{cut} is the cut-off energy.

$$\phi(E) = \phi_o \left(\frac{E}{E_o}\right)^{-\alpha-\beta log(\frac{E}{E_o})} \exp\left(\frac{-E}{E_{cut}}\right) \quad (\textbf{ECLP}) \tag{2.3}$$

$$\phi(E) = \phi_o \left(\frac{E}{E_o}\right)^{-\alpha-\beta log(\frac{E}{E_o})} \quad (\textbf{LP}) \tag{2.4}$$

where α and β are power and log indices respectively.

$$\phi(E) = \phi_o \times \begin{cases} \left(\frac{E}{E_b}\right)^{\gamma_1} & \text{if } E < E_b \\ \left(\frac{E}{E_b}\right)^{\gamma_2} & \text{otherwise} \end{cases} \quad (\textbf{BPL}) \tag{2.5}$$

where E_b is the break energy and γ_1 and γ_2 are the power indices.

Using the `Gammapy` spectral model, the first source that was treated was 4FGL J0232.8+2018 (1ES 0229+200). This blazar is frequently used in studying the characteristics of extreme blazars as it is a high frequency peaked BL Lac object and with a hard spectrum extending to 10 TeV. The data for the source was taken from the 4FGL catalog available in `Gammapy`. In this data, the highest detected energy point is at 0.05 TeV. In order to extrapolate the spectrum to higher energies, we also included the data from MAGIC which detects the source up to 3.69 TeV. Since our goal was to search for ALP signatures in the high energy spectrum region, the data points were fitted and extrapolated using the test functions [2.1 - 2.5]. Fig. 2.4 shows the fit that was performed using the exponential cut-off log-parabola as a fit function on the intrinsic points. The intrinsic points were computed by deconvolution of the observed points by EBL that is obtained from the Dominguez model [35] for the respective redshift of the source (for 1ES 0229+200 it is z = 0.14). The corresponding energy of the last point of the source data that was obtained from MAGIC at 3.69 TeV was chosen to be the cut-off value for the fit function.

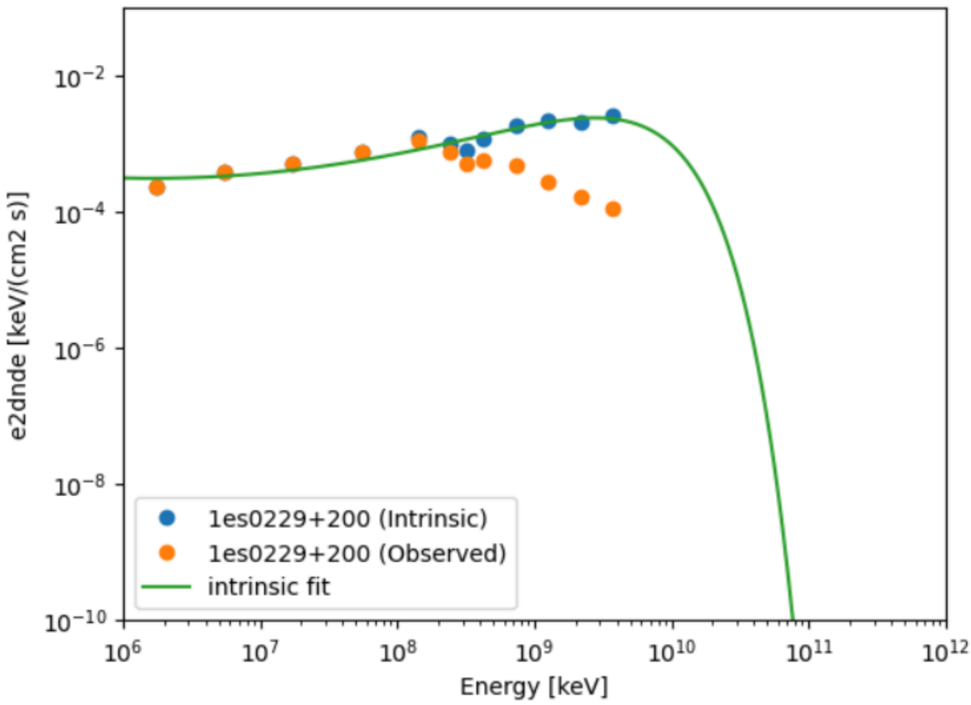

Figure 2.4: Extrapolated Spectrum for 1ES 0229+200 using Log-parabola with the Exponential Cut-off

In the case of 1ES 0229+200, the fit results were good with the R-squared value of 0.9. Since we wanted to do the analysis for more sources, the same process was done for few other strong sources available in 4FGL catalog but we did not get satisfactory fit results these times. One reason was that all of the sources cannot be modelled or fit with the same test function. We were looking for more generic method of fitting that can be applied to the flux data of all the sources. But this was not possible here as we had to look for the shape of the spectrum and then decide which function would provide the optimum fit. Secondly, in order to apply the fit using the mathematical functions, input of some initial fit parameters such as power-law indices or pivot energy is required. The issue here was that even the minor changes in these input parameters could fail the fit and we need more generic/automatic way to extrapolate the large number of sources.

2.4 Multiwavelength Data - Firmamento

Considering the above mentioned issues in the fit of the sources with `Gammapy` on the LAT data, we decided to model the complete multiwavelength SED of the sources. Multiwavelength photon spectra can be modelled by particle radiative processes that occur in AGN jets. We started with the hardest and the most intense blazar sources from 3FHL catalog as shown in Fig. 2.3. Multiwavelength blazar data besides Fermi-LAT was accessed using Firmamento [72] which is an online multiwavelength data platform dedicated to blazars and multimessenger sources. It provides access to currently released astronomical data and visuals from high energy surveys of the sources. Fig. 2.5 shows the multiwavelength data accessed from firmamento for the source Markarian 421 collected from various instruments/catalogs. The data can be downloaded in csv format as shown in Fig. 2.6.

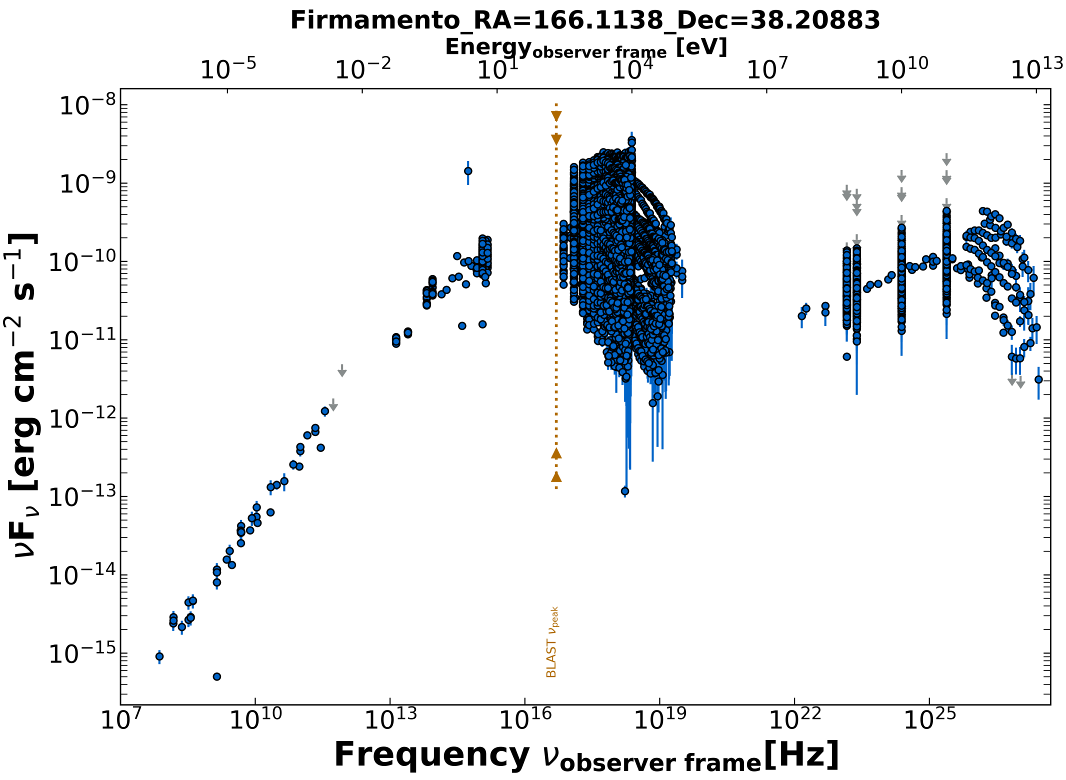

Figure 2.5: Multifrequency data for Mkn421 accessed from firmamento [72]

Photons that are emitted from the blazar source in Fig. 2.5 are produced by different radiative processes in AGN. These processes can mainly be categorized into Leptonic and Hadronic models. The multiwavelength SED is divided into two parts. The low energy part is attributed to the synchrotron radiation from electrons or positrons. Synchrotron radiation occurs in the Leptonic model and can be defined as the radiation emitted by the charged particle traversing in the magnetic field. The high energy part is more ambiguous but usually attributed to inverse Compton scattering of high energy electrons. When synchrotron photons interacts with the same electron population that generated them via inverse Compton, this scenario is called Synchrotron Self Compton (SSC). Generally, BL Lac objects are modelled with SSC process [13]. Fig. 2.7 shows a rough illustration of radiative processes involved in AGNs including pion decay which usually occurs in high energy part of SED after hadronic interactions.

freq	flux	err_flux	MJD_start	MJD_end	flag	catalog	reference
8.87E+08	2.98E-16	2.66E-17	55000	55000		RACS	Hale et al. 2021 PASA 38 e058
1.40E+09	2.59E-16	9.80E-18	55000	55000		NVSS	Condon et al. 1998 AJ 115 1693
3.00E+09	6.52E-16	7.35E-18	55000	55000		VLASSQL	Gordon et al. 2021 ApJS 255 30
1.36E+13	2.19E-12	4.88E-13	55368.09	55368.09		WISEME	Wright et al. 2010 AJ 140 1868
1.36E+13	1.19E-12	4.12E-13	55367.96	55367.96		WISEME	Wright et al. 2010 AJ 140 1868
1.36E+13	2.37E-12	3.97E-13	55368.16	55368.16		WISEME	Wright et al. 2010 AJ 140 1868
1.36E+13	9.09E-13	4.22E-13	55367.89	55367.89		WISEME	Wright et al. 2010 AJ 140 1868
1.36E+13	1.26E-12	4.42E-13	55368.16	55368.16		WISEME	Wright et al. 2010 AJ 140 1868
1.36E+13	1.51E-12	4.31E-13	55368.23	55368.23		WISEME	Wright et al. 2010 AJ 140 1868
1.36E+13	1.16E-12	4.46E-13	55368.03	55368.03		WISEME	Wright et al. 2010 AJ 140 1868
1.36E+13	1.12E-12	3.95E-13	55368.29	55368.29		WISEME	Wright et al. 2010 AJ 140 1868
1.36E+13	1.34E-12	5.10E-13	55368.29	55368.29		WISEME	Wright et al. 2010 AJ 140 1868
1.36E+13	1.13E-12	4.12E-13	55367.63	55367.63		WISEME	Wright et al. 2010 AJ 140 1868
2.50E+13	1.60E-12	1.36E-13	55368.03	55368.03		WISEME	Wright et al. 2010 AJ 140 1868
2.50E+13	1.83E-12	1.27E-13	55368.29	55368.29		WISEME	Wright et al. 2010 AJ 140 1868
2.50E+13	1.60E-12	1.31E-13	55368.16	55368.16		WISEME	Wright et al. 2010 AJ 140 1868
2.50E+13	1.63E-12	1.31E-13	55368.36	55368.36		WISEME	Wright et al. 2010 AJ 140 1868
2.50E+13	1.74E-12	1.25E-13	55368.16	55368.16		WISEME	Wright et al. 2010 AJ 140 1868
2.50E+13	1.68E-12	1.19E-13	55368.49	55368.49		WISEME	Wright et al. 2010 AJ 140 1868
2.50E+13	1.63E-12	1.19E-13	55368.09	55368.09		WISEME	Wright et al. 2010 AJ 140 1868
2.50E+13	1.68E-12	1.18E-13	55368.62	55368.62		WISEME	Wright et al. 2010 AJ 140 1868
2.50E+13	1.66E-12	1.20E-13	55368.23	55368.23		WISEME	Wright et al. 2010 AJ 140 1868

Figure 2.6: Multifrequency data for Mkn421 in csv format accessed from firmamento

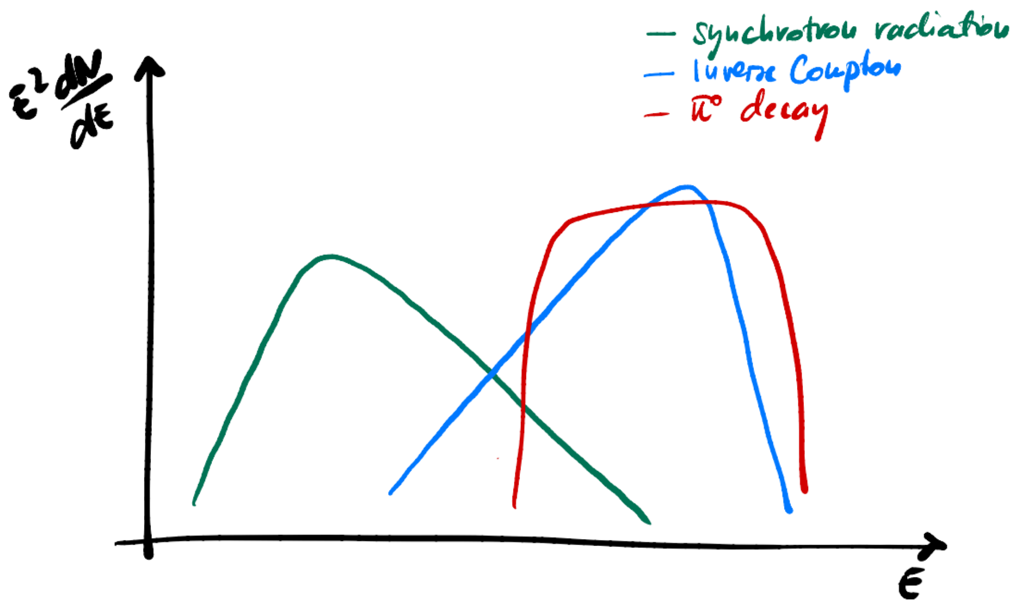

Figure 2.7: Illustration of low and high energy processes involved in AGN

2.5 SED Data Cleaning and Intrinsic Spectra

Once we have the multiwavelength data for all our selected blazar sources, the next step before modelling the SED (as shown in Fig. 2.5) is to clean the data and to prepare it for the modelling. It is important to do the overview on the data and remove the unwanted data. In the multiwavelength data, there are some points with a flag "UL" (upper limit). Since we are interested in modelling the weighted average of the flux points and the data points that we are working with already have an associated flux error, we are not including the upper limits in our analysis. Also, in this study we are using MMDC platform (discussed in next section) to model the sources and at this time MMDC does not support the upper limits in the multiwavelength data. Secondly, there is some data from catalogs that are not necessary to include in our analysis. For instance, the catalogs that we removed from our data include NEOWISE, WISEME, WISE and 2BIGB especially because these catalogs have a lot of data points in low energy range around $\sim 10^{13}$ Hz. One reason to remove these catalogs is that 2BIGB is just the another Fermi analysis and we already have data from other Fermi catalogs. We also removed NEOWISE, WISEME and WISE as these catalogs are the average of UNWISE which is yet another catalog included in our data. Usually, the radio and lower frequency data is excluded while modelling the blazar source as the emission in these bands is due to the self-absorption [73]. Self-absorption occurs when the electron absorbs a synchrotron photon emitted by another electron. Removing the unwanted data is still not enough to perform the multiwavelength modelling as there are few other issues as well. One is that the multiwavelength data of blazars is highly variable. This variability can range from few minutes to several years with a variation in the magnitude of the flux of the blazar between its low and active states. This variability can be observed over the entire multiwavelength spectrum [74]. Second problem is that we have the multiwavelength data from different catalogs/instruments which creates multiple flux points for the same frequency (energy). And lastly, the data from some of the sources contains contribution from the galaxy besides the jet. This contribution arises from the stellar emission due to the galaxy hosting a blazar source. It is dominant at UV/optical energies and its flux measurements are higher than the non-thermal emission of jet predicted by the SSC model [75].

In order to remove multiple points with the same frequency, we decided to compute the weighted average of those points. The weighted average is calculated based on the errors associated with each data point. Now, this method may not be a very good estimate to get rid of the flux data with variable states. One method to deal with this issue can be adaptive binning of the flux points that was explored marginally in this study. Once we have the weighted averaged points for the source, the last step before modelling the SED is to compute the intrinsic spectra. The reason we want to model the intrinsic spectra and not the observed spectra is because while computing the ALP analysis, `GammaALPs` includes the EBL contribution in the propagation function. Therefore, the intrinsic points were computed by deconvolution of the observed weighted averaged points by EBL that is obtained from the Dominguez 2011 model for the respective redshift of the source. Following plots illustrate the process of performing the weighted for the source 3FHL J0449.4-4350. Fig. 2.8 shows the data for the source downloaded from Firmamento and Fig. 2.9 shows the computed weighted averaged points and observed and intrinsic points for this source. It can be seen that EBL attenuation becomes significant only at higher energies.

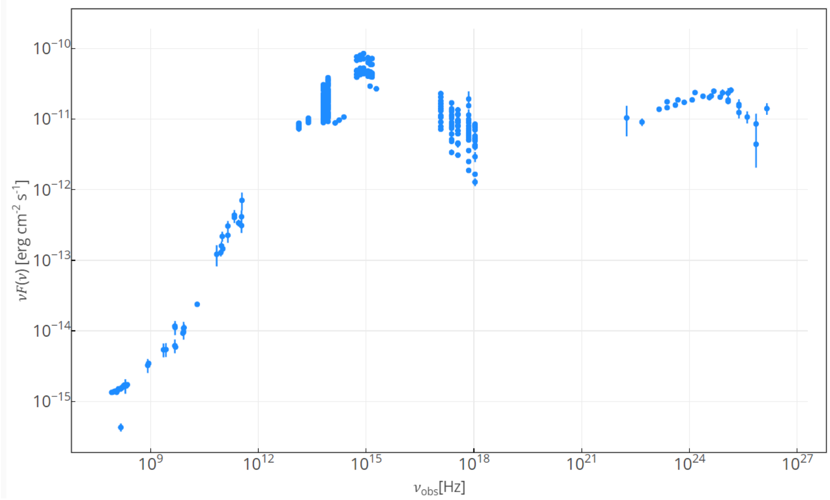

Figure 2.8: Multiwavelength data for 3FHL J0449.4-4350 downloaded from Firmamento

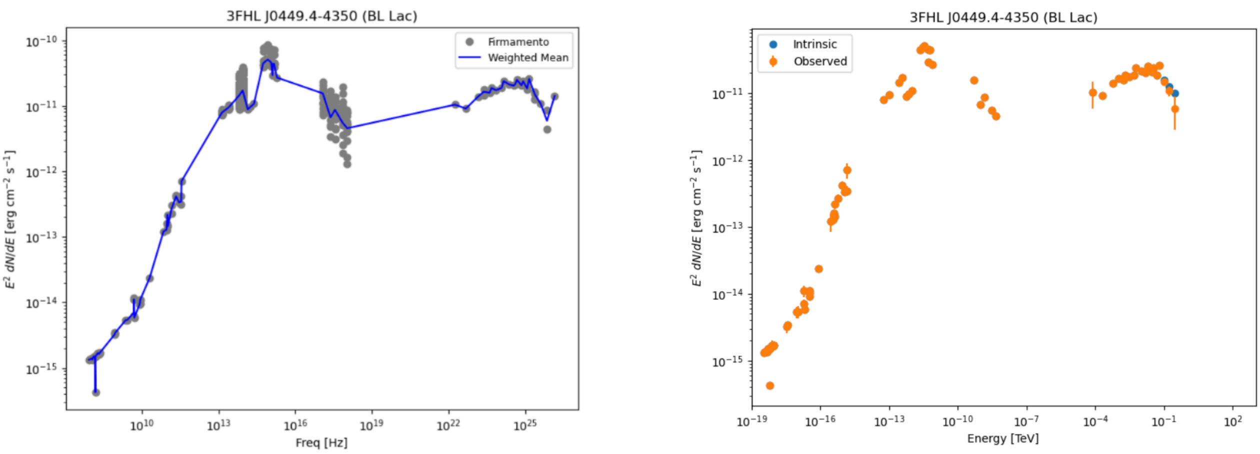

(a) Weighted average Data

(b) Intrinsic and Observed SED

Figure 2.9: Blazar Source 3FHL J0449.4-4350

2.6 Multiwavelength Data Modelling with Markarian Multiwavelength Data Center (MMDC) and AGNPY

Once we have the intrinsic spectral points for the sources, the next step is to model the multiwavelength SED as we wanted an extrapolated spectra to SWGO energies on which ALP analysis can be applied. `Agnpy` [76] is a model-fitter which focuses on numerical computation of photon spectra produced by particle radiative processes in AGN jets. It provides ways for modelling the photon spectra with SSC or External Compton (EC) model and performs the fit using techniques including Gammapy (Chi-squared method) and Monte Carlo Markov Chain (MCMC). `Agnpy` uses already defined spectral model of SSC to perform the fit but the electron distribution has to be defined explicitly using the broken power law (BPL) function (Eq.2.5). Moreover, some parameters of SSC model and emission region including the Doppler factor, value of magnetic field and the time variablity have to be input manually. Also, the model parameters of BPL such as two power indices and minimum and maximum Lorentz factors have to be input by the user. We first tested the `Agnpy` tutorial for the Mkn 421 data with the multiwavelength data already given by `Agnpy` and it gave perfect fit results as shown in Fig. 2.10. Later when we tried to perform the fit with χ^2 method for few other blazar sources that we selected for our analysis, fitting completely failed. We also tried to run the fit using MCMC but fitting failed again. One reason can be that the `Agnpy` fitter is very sensitive to the initial input parameter values. Even the slightest change in the values can fail the fit. Secondly, as we discussed in the previous section, multiwavelength data can be highly variable and can involve different states. Therefore `Agnpy` is unable to perform a good fit for such data. Fig. 2.11 shows the fit results using χ^2 minimization for the source 3FHL J0033.5-1921. It can be seen that the fit is not working.

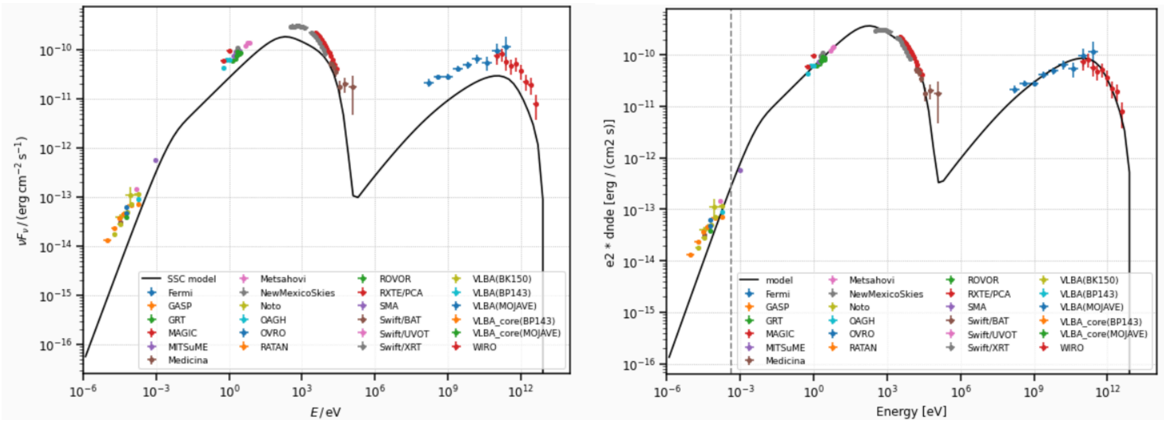

(a) Before Fit (Initially predicted SSC model) (b) After Fit (Optimized SSC model)

Figure 2.10: Mrk 421 data fitting with AGNPY

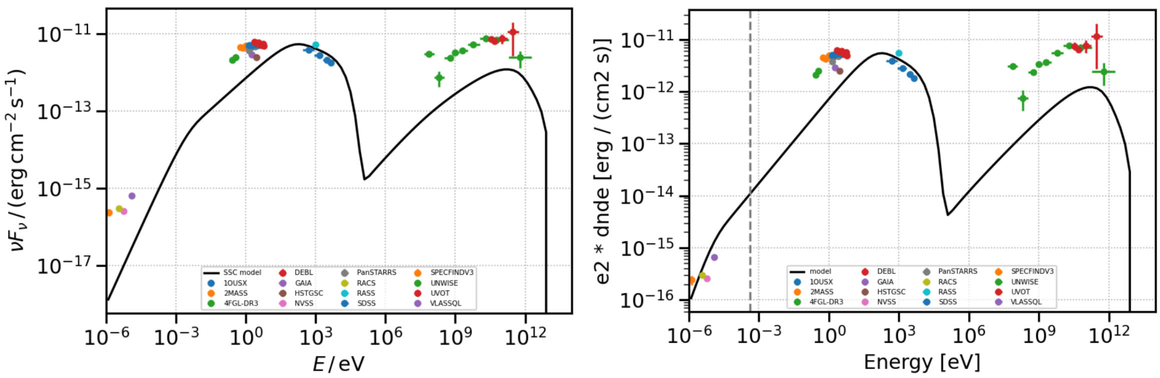

(a) Before Fit (Initially predicted SSC model) (b) After Fit (Optimized SSC model)

Figure 2.11: 3FHL J0033.5-1921 data fitting with AGNPY

Finally, we decided to model the SEDs using MMDC as an alternative to `Agnpy` [73]. It is an online web-based platform for building and analyzing multiwavelength SEDs. It performs the blazar modelling using Convolutional Neural Networks (CNN) technique. Like `Agnpy`, MMDC also uses SSC process to model BLL objects. On the website, it only requires to upload the csv file for the data including three columns namely frequency, flux and flux error for modelling. Unlike `Agnpy`, MMDC does not require to input any model or emission region parameters except redshift. It initiates and optimizes all the other parameters by itself. Fig. 2.12 shows an illustration of a fit performed by MMDC on the source 3FHL J1221.3+3010. Best model parameters determined by MMDC after the fit are also shown on the right side of the Fig. 2.12. After the fit, we can download the best fit parameters and corner plots along with the best model. Fit parameters are the parameters of SSC model and are shown in Table 2.3. In the model, it is assumed that the emission region (also called Blob) is spherical with a comoving radius R and moving with Lorentz factor γ. Other parameters include Doppler boost factor δ, homogenous and constant magnetic field B, and electron luminosity L_e obtained from electron injection function Q_e which is assumed to be a cut-off power law with spectral index p [73].

Parameter	Symbol	Units	Min. value	Max. value
Blob Radius	R	cm	10^{15}	10^{18}
Doppler Boost	δ	-	3	50
Min. Lorentz Factor	γ_{min}	-	$10^{1.5}$	10^{5}
Cutoff Lorentz Factor	γ_c	-	10^{2}	10^{8}
Electron Luminosity	L_e	ergs s^{-1}	10^{42}	10^{48}
Magnetic Field	B	Gauss	10^{-3}	10^{2}
Spectral Index	p	-	1.8	5

Table 2.3: Characteristics of SSC model parameters used in MMDC modelling [73]

MMDC is also sensitive to inconsistent data and gives an error if data is variable or contains too many outliers. For our selected blazar sources, it performed good fit, but in some cases where data was highly variable or the data points were less, the fit results were not satisfactory. For instance, Fig. 2.13 shows the fit results for the sources 3FHL J0818.2+4222 and 3FHL J0433.6+2905. It can be seen that the fit is not working perfectly. Therefore, we proceeded with the sources for which we got a good fit from MMDC and then we applied the ALP analysis on those sources. The fit results for all the sources are shown in chapter 3.

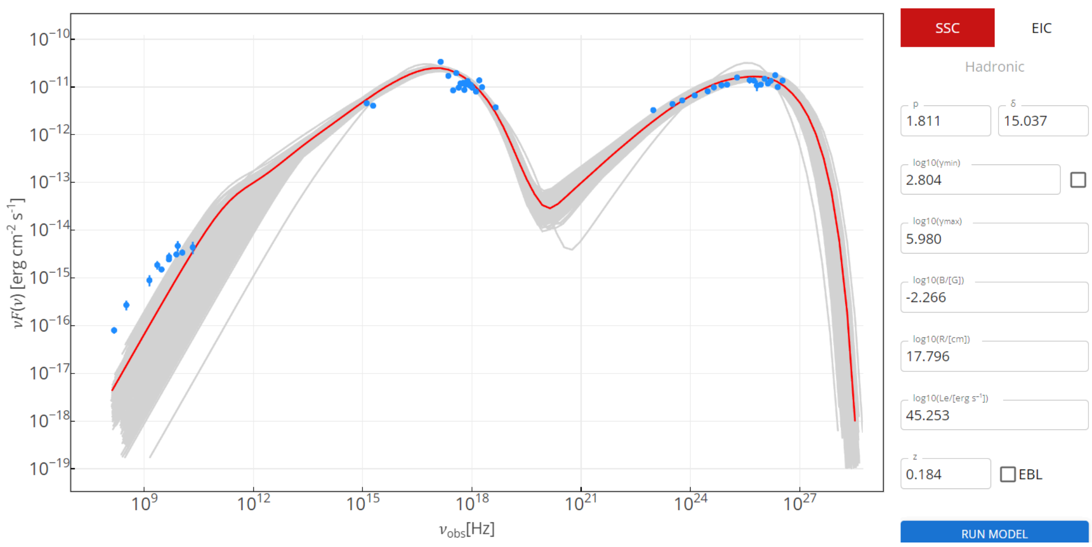

Figure 2.12: MMDC modelling for 3FHL J1221.3+3010

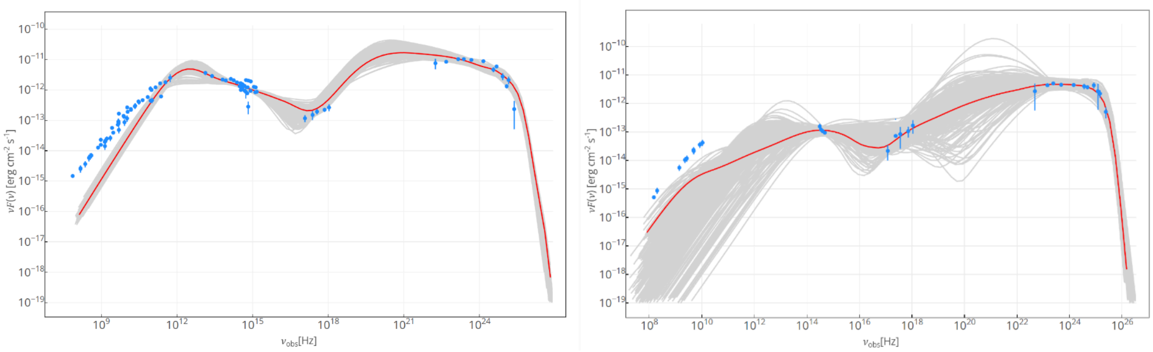

(a) 3FHL J0818.2+4222 (b) 3FHL J0433.6+2905

Figure 2.13: Modelling of the sources with MMDC showing bad fitting. Red curve represents the fit model with best parameters while the grey spectra represents the random samples generated by MMDC using CNN. (a). The fitting curve does not include the X-rays points (around 10^{18} Hz) resulting in a bad fit. (b). It is clear that the fitting curve completely fails to represent the SSC model shape.

2.7 ALP Modelling using GammaALPs

The final step is to apply the ALP model on the spectra in order to predict the effect in the spectra due to photon-ALP conversion at higher energies. `GammaALPs` [31] is a python package that can be used to provide the calculation of mixing probability between ALPs and photons in various astrophysical environments and magnetic field models. There are various tutorials available on the `GammaALPs` website but the one which we used is the photon-ALP mixing in AGN jet with helical and tangled magnetic field. There are not many studies available on the nature of magnetic fields of AGN jets and considering the limited scope of this study, it was not feasible to explore it and therefore this assumption was taken as valid for all the blazars under consideration. The values used by `GammaALPs` for the jet parameters are taken from the best fit values determined in Potter & Cotter model (2015) [77]. The ALP model consists of three propagation functions. First function is defined for a jet magnetic field when beam is propagating inside the ultra-relativistic jet, second propagation function is defined for EBL attenuation in the intergalactic medium which comes after the beam has left the jet or cluster in case of . Third function is defined for Galactic magnetic field when the beam has entered the Milky Way. In our analysis we have neglected the contribution from IGMF because its affect is almost negligible as we already discussed in chapter 1. Now, the total photon survival probability can be calculated by providing the redshift of the source and the parameters of the ALPs which are mass m_a and coupling to photons $g_{a\gamma}$. Fig. 2.14 illustrates the total photon survival probability computed for the source 3FHL J0449.4-4350 for four different ALP masses and coupling of $g_{a\gamma} = 1 \times 10^{-10}$ GeV^{-1} and $g_{a\gamma} = 1 \times 10^{-11}$ GeV^{-1} respectively.

Once we have computed the photon survival probability for different ALP masses and coupling, we can apply these ALP models on the intrinsic spectra of the source by first interpolating the photon survival probability on the energy points of the intrinsic spectra and then simply multiply the ALP models with the intrinsic best fit model that we obtained with MMDC. The final plots that we obtained for each blazar source after the complete analysis are discussed in chapter 3.

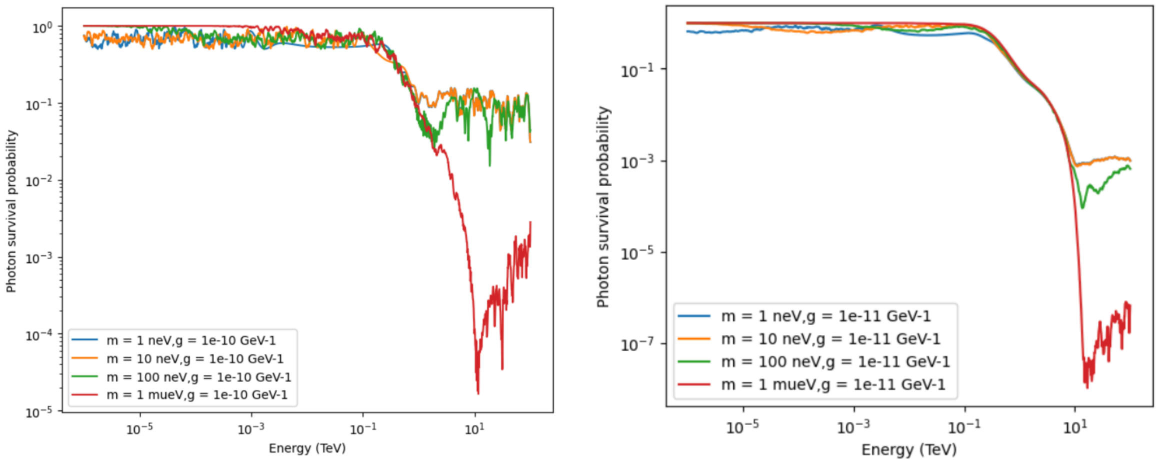

Figure 2.14: Total Photon Survival Probability for 3FHL J0449.4-4350 (z = 0.205) with $g_{a\gamma} = 1 \times 10^{-10}$ GeV^{-1} and $g_{a\gamma} = 1 \times 10^{-11}$ GeV^{-1}

Chapter 3
Results

As discussed in chapter 2, we selected around 30 blazar sources from the 3FHL catalog and modelled their multiwavelength spectra with MMDC. In this chapter, we are going to discuss the sources for which we got the good fitting and we applied the ALP analysis on them. We will discuss 12 sources in detail including their spectral properties, multiwavelength spectra, EBL attenuation, SSC best fit model and parameters, and finally the plots with and without ALP models. Table 3.1 shows the basic information and the spectral properties for all the BLL sources that are analyzed.

Source	**Redshift**	**Best Intrinsic Fit Function**	**Power law (PL) spectral index**	**Pivot energy (GeV)**	**Flux Density (GeV^{-1} cm^{-2} s^{-1})**
3FHL J0449.4-4350	0.205	Power law (PL)	2.2	22.9	2.47e-11
3FHL J0630.9-2406	1.238	LogParabola (LP)	2.4	16.6	2.51e-11
3FHL J0738.1+1742	0.424	Power law (PL)	2.6	18.4	1.67e-11
3FHL J1217.9+3006	0.130	Power law (PL)	2.2	22.1	1.59e-11
3FHL J1230.2+2517	0.135	Power law (PL)	2.6	18.0	7.84e-12
3FHL J1959.9+6508	0.047	Power law (PL)	1.9	28.2	1.07e-11
3FHL J2158.8-3013	0.116	LogParabola (LP)	2.1	18.3	7.71e-11
3FHL J0809.8+5218	0.138	Power law (PL)	2.2	22.6	1.01e-11
3FHL J1015.0+4926	0.212	Power law (PL)	2.1	23.7	1.96e-11
3FHL J0650.7+2503	0.203	LogParabola (LP)	1.8	22.6	9.56e-12
3FHL J0033.5-1921	0.610	Power law (PL)	2.2	23.1	8.36e-12
3FHL J1243.2+3627	1.065	Power law (PL)	2.2	23.0	6.21e-12

Table 3.1: Spectral Properties of selected BLL sources. Columns represent, (1). Official source name 3FHL JHHMM.m+DDMM, (2). Redshift (distance) of the source, (3). Spectral type (Power Law or Log Parabola), (4). Best-fit photon number index when fitting with power law, (5). Energy at which error on differential flux is minimal, (6). Differential flux at Pivot Energy [65].

3.1 Multiwavelength Photon Spectra

Multiwavelength data for the sources was accessed using Firmamento and MMDC. The data was downloaded using the counterpart name and not the source (3FHL) name. Following Figs.[3.1 & 3.2] show the multiwavelength data for all 12 sources. From the plots, it can be seen that the x-ray and gamma-ray region has a lot of multiple data points and outliers as discussed in chapter 2 in section 2.5. Therefore, we have computed the weighted average of the points in order to model the SED for this study.

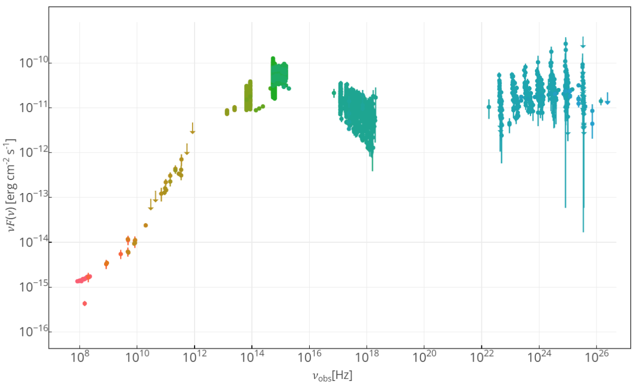

(a) 3FHL J0449.4-4350

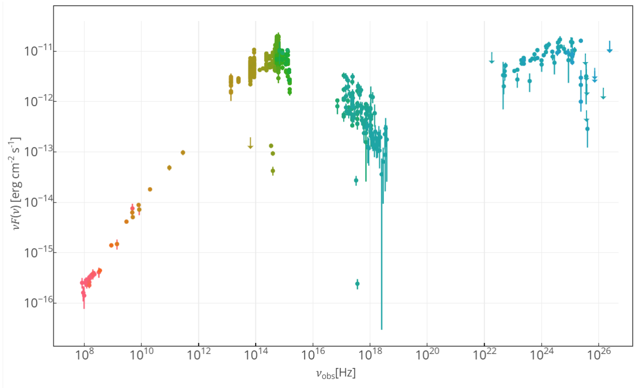

(b) 3FHL J0630.9-2406

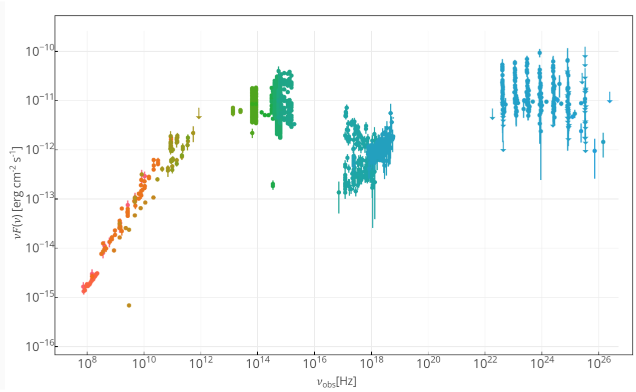

(c) 3FHL J0738.1+1742

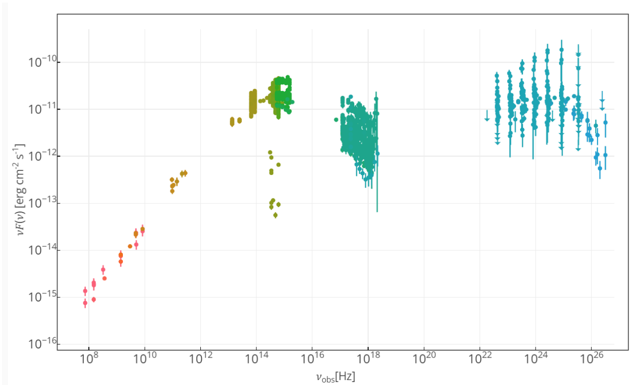

(d) 3FHL J1217.9+3006

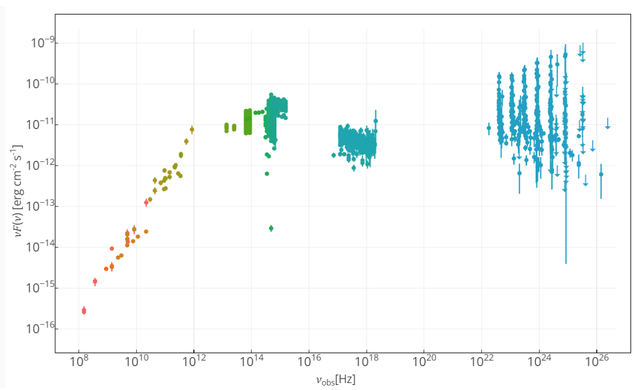

(e) 3FHL J1230.2+2517

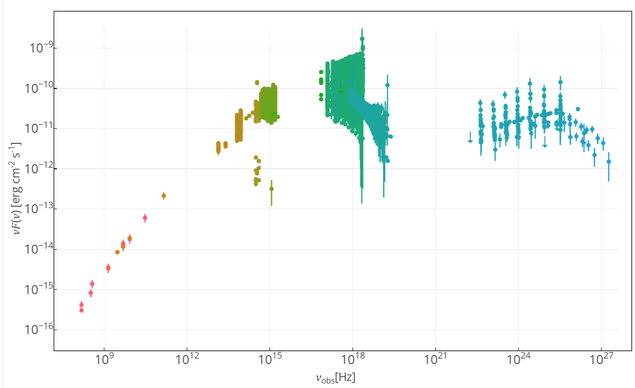

(f) 3FHL J1959.9+6508

Figure 3.1: Multiwavelength data of blazar sources

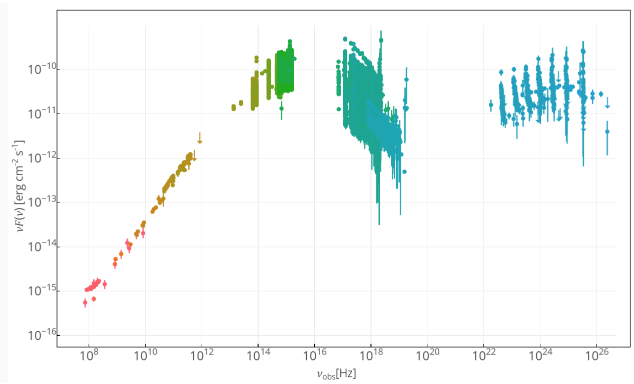

(a) 3FHL J2158.8-3013

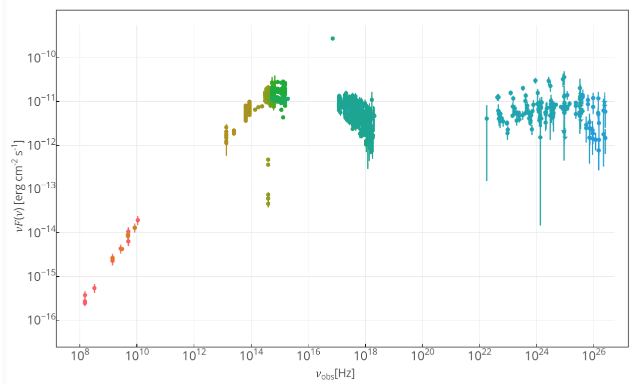

(b) 3FHL J0809.8+5218

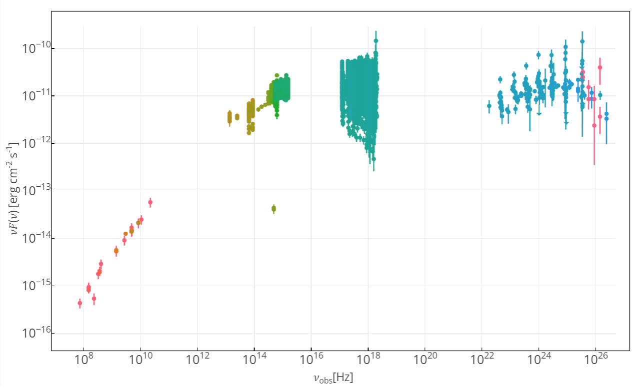

(c) 3FHL J1015.0+4926

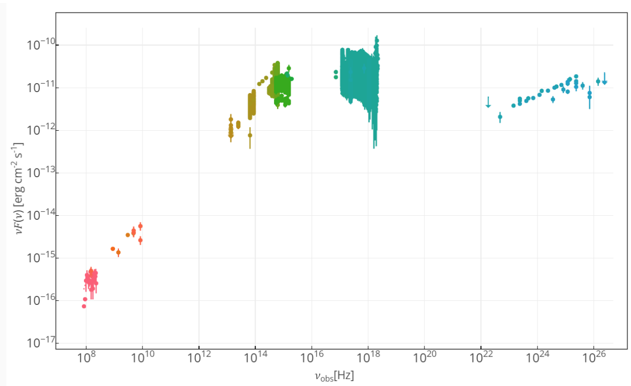

(d) 3FHL J0650.7+2503

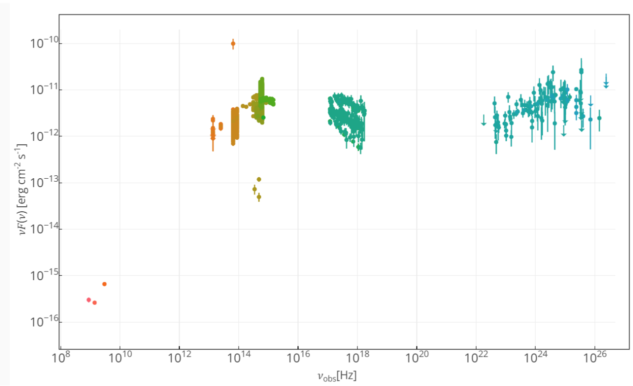

(e) 3FHL J0033.5-1921

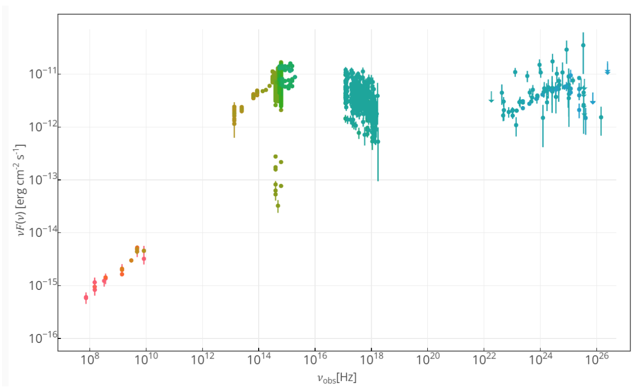

(f) 3FHL J1243.2+3627

Figure 3.2: Multiwavelength data of blazar sources

3.2 EBL Attenuation

In order to compute the intrinsic spectra, EBL attenuation is obtained for all the sources as shown in the following Fig. 3.3. EBL attenuation is computed for each source using the Dominguez model [35] as discussed in chapter 1. It is evident from the plot that for the source 3FHL J0630.9-2406 and 3FHL J1243.2+3627 with redshift 1.238 and 1.065 respectively, the EBL attenuation is steeply falling even before 1 TeV. The closest source that we have is 3FHL J1959.9+6508 at z = 0.047 and it can be seen in Fig. 3.3 that the EBL attenuation for this source becomes dominant after 20 TeV.

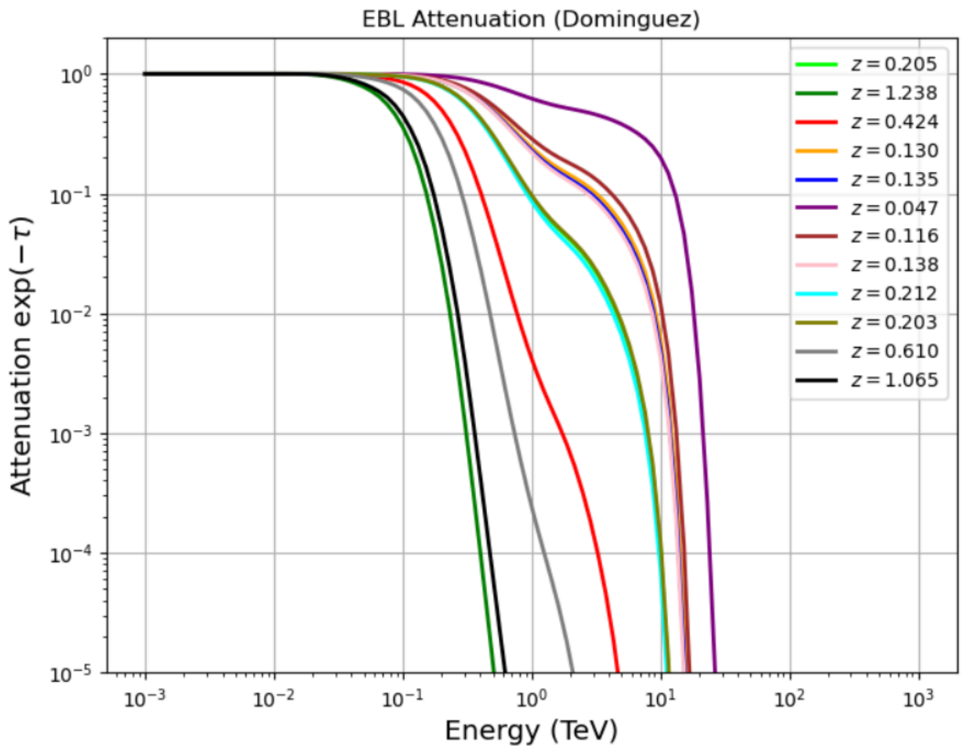

Figure 3.3: EBL attenuation for all the sources computed using Dominguez Model [35]

3.3 MMDC Model and Best Parameters

The Intrinsic SED of all the sources is modelled using MMDC as shown in the following Figs.[3.4 & 3.5]. The best fit parameters as discussed in chapter 2 (Table 2.3) are also obtained from MMDC for the sources and are shown in Table[3.2 & 3.3].

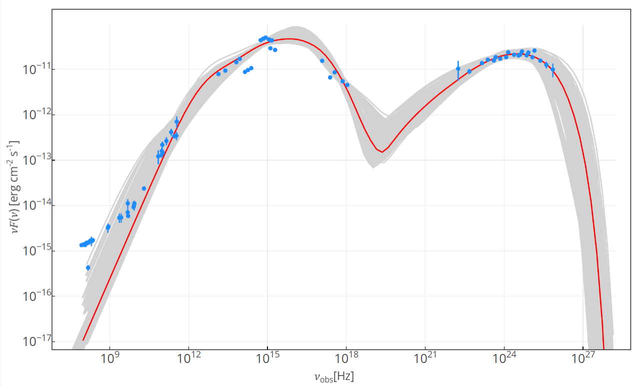

(a) 3FHL J0449.4-4350

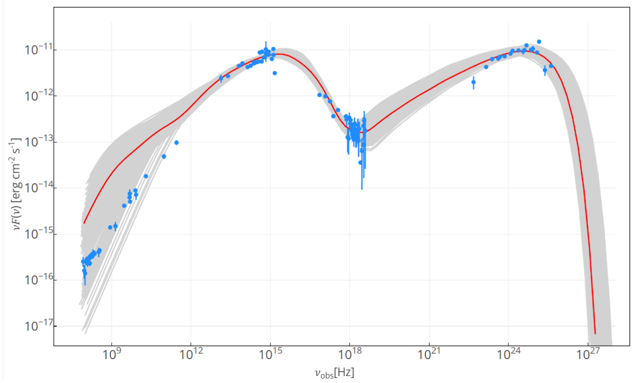

(b) 3FHL J0630.9-2406

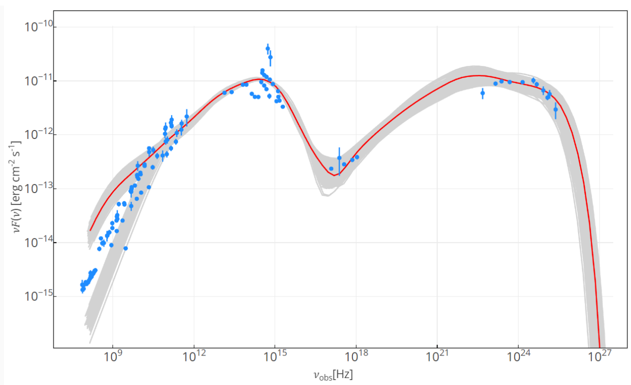

(c) 3FHL J0738.1+1742

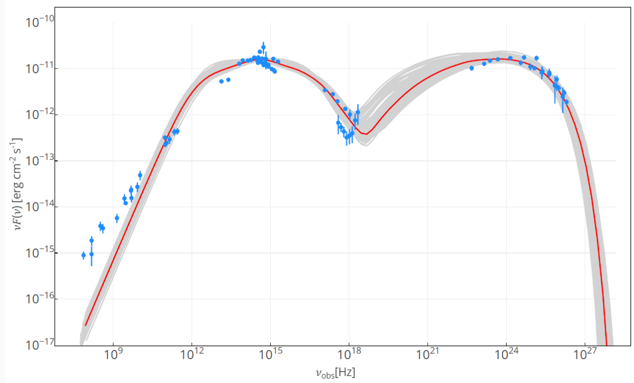

(d) 3FHL J1217.9+3006

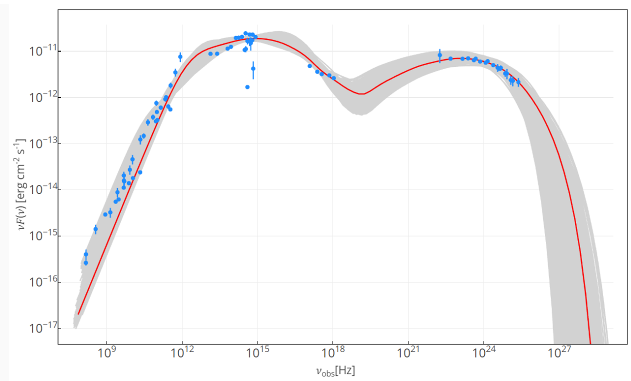

(e) 3FHL J1230.2+2517

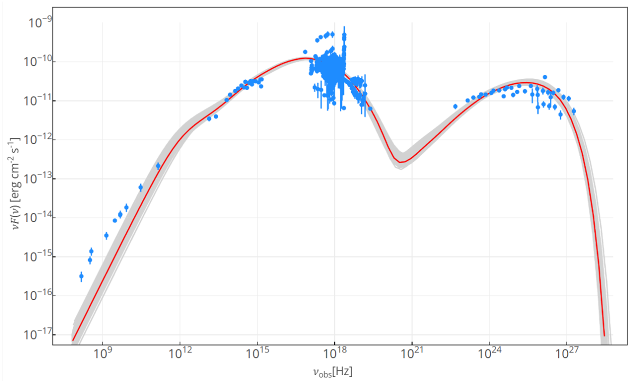

(f) 3FHL J1959.9+6508

Figure 3.4: Modelling of the sources with MMDC

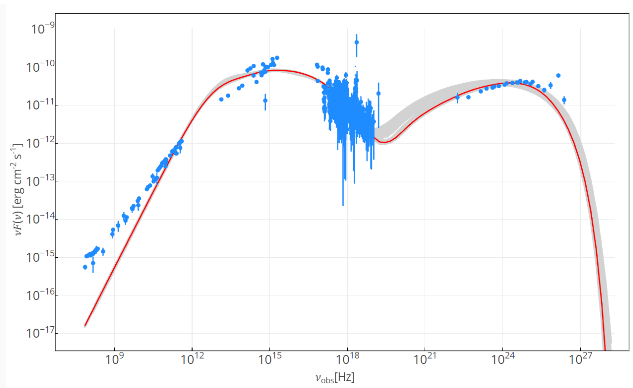

(a) 3FHL J2158.8-3013

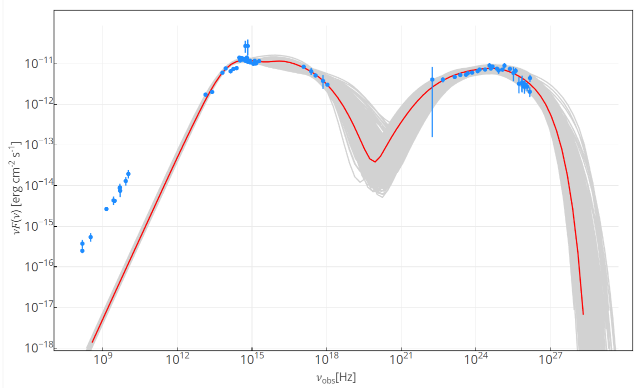

(b) 3FHL J0809.8+5218

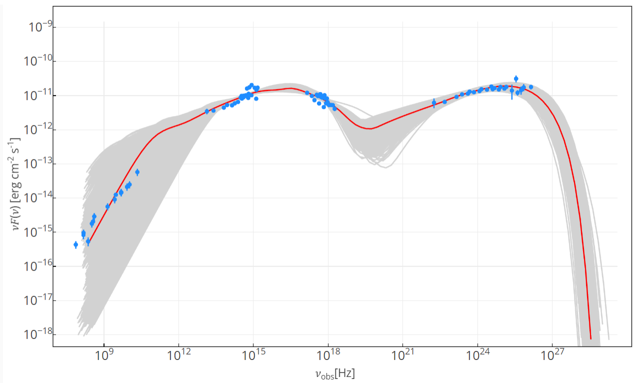

(c) 3FHL J1015.0+4926

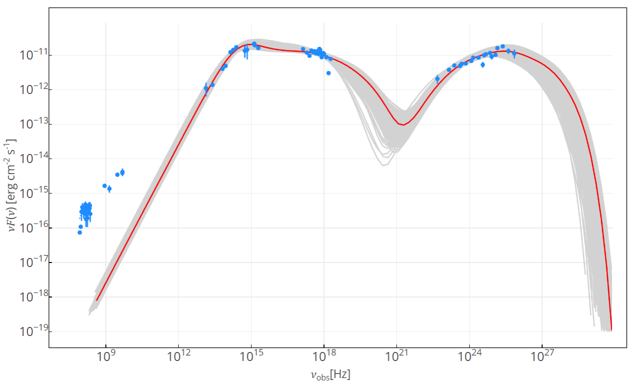

(d) 3FHL J0650.7+2503

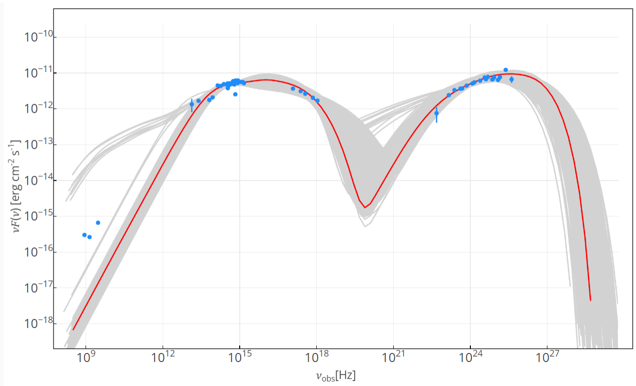

(e) 3FHL J0033.5-1921

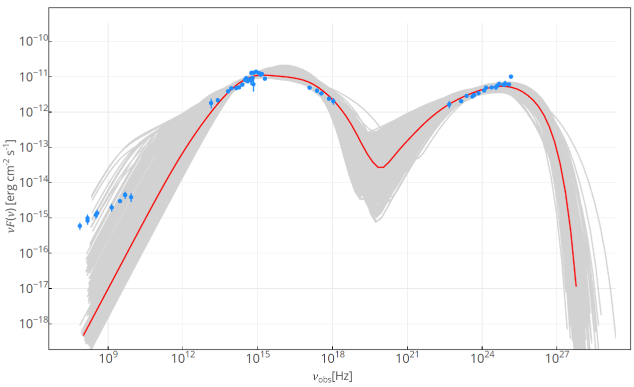

(f) 3FHL J1243.2+3627

Figure 3.5: Modelling of the sources with MMDC

Parameter	3FHL J0449.4-4350	3FHL J0630.9-2406	3FHL J0738.1+1742	3FHL J1217.9+3006	3FHL J1230.2+2517	3FHL J1959.9+6508
Log(B)	-1.82	-1.69	-2.71	-2.01	-1.21	-2.01
Log(L_e)	44.27	45.49	46.39	44.33	43.79	43.83
Log(γ_c)	5.56	5.02	4.61	5.76	6.44	6.31
Log(γ_{min})	3.19	1.50	1.50	3.16	2.94	3.16
Log(R)	17.79	17.48	17.79	17.56	17.32	17.77
δ	11.12	19.37	20.00	9.41	8.07	7.05
p	2.11	2.00	1.89	2.68	2.60	1.93

Table 3.2: SSC best model parameters obtained from MMDC

Parameter	3FHL J2158.8-3013	3FHL J0809.8+5218	3FHL J1015.0+4926	3FHL J0650.7+2503	3FHL J0033.5-1921	3FHL J1243.2+3627
Log(B)	-1.48	-1.51	-1.88	-2.45	-2.72	-1.22
Log(L_e)	44.13	43.19	45.08	44.68	45.38	46.02
Log(γ_c)	5.86	5.62	5.84	6.98	4.07	5.58
Log(γ_{min})	3.30	3.53	2.31	4.16	4.07	3.92
Log(R)	17.79	15.71	17.12	17.39	17.79	17.79
δ	7.84	40.84	27.02	48.10	49.23	20.55
p	2.23	3.07	2.40	3.04	2.65	1.90

Table 3.3: SSC best model parameters obtained from MMDC

3.4 Simulated Spectra with ALP models

After the modelling of the SED, ALP models are applied on the spectra for four different ALP masses to observe the change in the spectra at higher energies as shown in the following Figs.[3.6 & 3.7]. These are the final plots of our study as here we complete our analysis. In the following plots, there are total six curves represented by different styles of a line. Four black colored lines represent the extrapolated flux of the source with four different ALP models. The four ALP models are with m_a = 1, 10, 100 neV and 1 μeV with photon-axion coupling $g_{a\gamma} = 1 \times 10^{-10}$ GeV^{-1}. The two red curves are extrapolated observed (solid line) and intrinsic (dashed line) flux of the source. Green points are the observed flux points and blue points are the intrinsic points (without the EBL attenuation). The grey shaded region is the SWGO sensitivity for 10 years.

There are various remarks that can be made by looking at these plots. First of all, the change in the observed flux due to ALPs at higher energies is prominent in some cases. Secondly, it can be seen that for a few sources such as 3FHL J0738.1+1742 and 3FHL J1230.2+2517, even with the ALP models, the flux falls below the SWGO sensitivity and hence these models of ALPs cannot be excluded with SWGO data of these sources. For most of the sources, it is also evident that the ALP models with mass 1 neV (solid line) and 10 neV (dash-dot line) almost have a same effect on the flux as these curves are indistinguishable. Moreover, these two ALP models (1 neV and 10 neV) are most likely to provide the gain in the flux as compare to higher ALP masses (100 neV or 1mueV). For instance, if ALPs really existed and if they alter the spectrum the way we think, the source 3FHL J0630.9-2406, can be detected with SWGO with the ALP model of 1neV. Moreover, the sources that are closer to us (low redshift), for instance, 3FHL J1959.9+6508 (z = 0.047), 3FHL J2158.8-3013 (z = 0.116) and 3FHL J1217.9+3006 (z = 0.130) can be detected with SWGO even if the ALPs does not exist and consequently no ALP-photon mixing occurs, as their observed spectra is above SWGO sensitivity.

Two sources 3FHL J0630.9-2406 and 3FHL J1243.2+3627 have higher redshifts 1.238 and 1.065 respectively and therefore they are only detected with ALPs if they exist satisfying the conditions of mass and coupling, otherwise their observed spectra falls below the SWGO sensitivity.

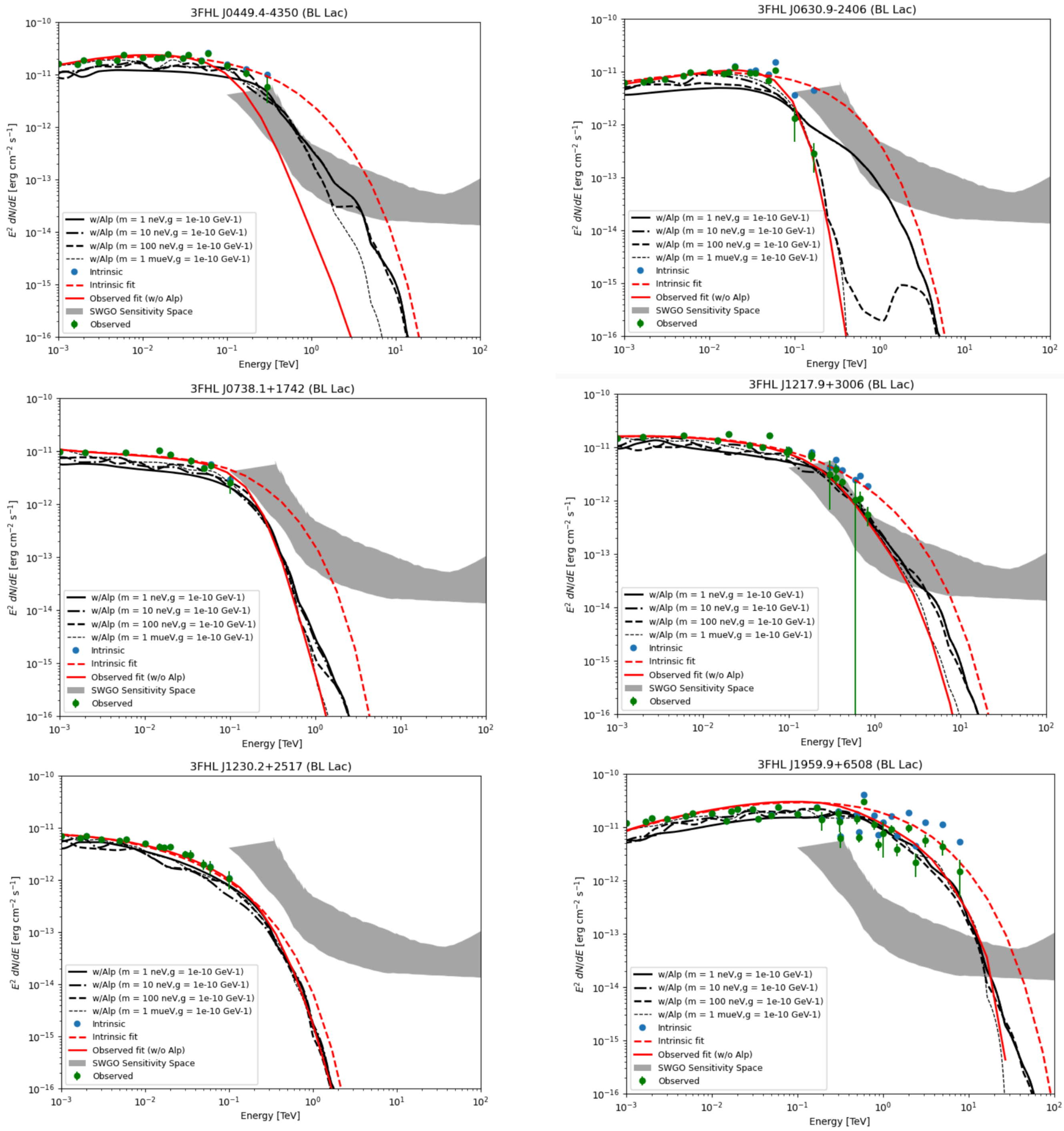

Figure 3.6: Simulated observed spectra (red line) and intrinsic spectra (red-dotted line). The flux with a contribution from ALPs has been simulated for four ALP masses (black curves). Grey shaded region represents SWGO sensitivity space.

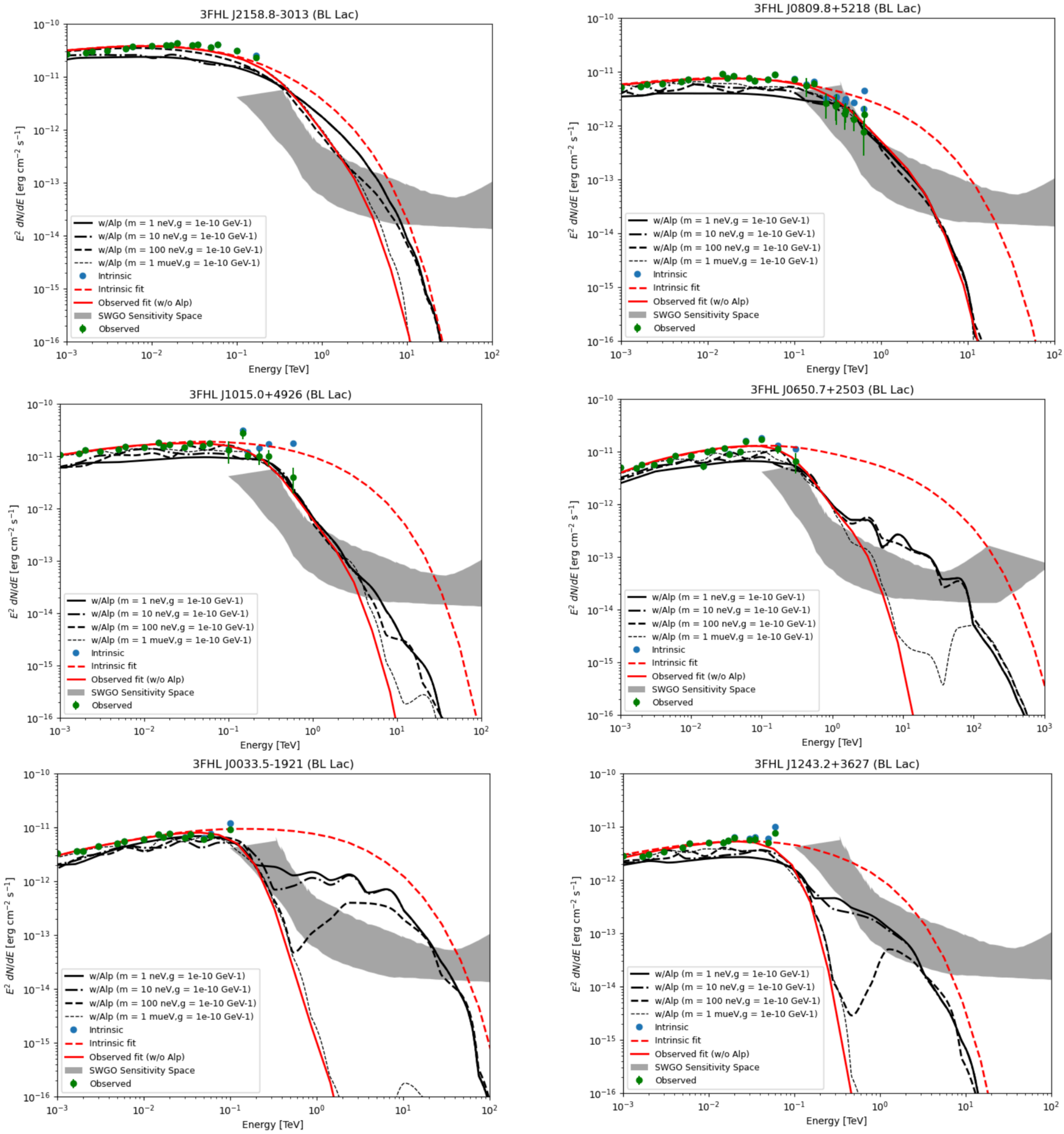

Figure 3.7: Simulated observed spectra (red line) and intrinsic spectra (red-dotted line). The flux with a contribution from ALPs has been simulated for four ALP masses (black curves). Grey shaded region represents SWGO sensitivity space.

3.5 ALP Parameter Space and SWGO Sensitivity Test

In the previous section, we simulated the spectra for four ALP models with masses 1neV, 10 neV, 100 neV, 1μeV and with photon-axion coupling $g_{a\gamma} = 1\times10^{-10}$ GeV^{-1}. One of the aims of our study is to explore the ALP parameter space and derive constraints on the ALP mass and coupling. In order to exclude the points in ALP parameter space at certain confidence level (CL), we need data from SWGO. Since, SWGO has not yet started collecting the data, it's not trivial to derive constraints on ALP parameters. Although, in order to explore the ALP parameter space and test the SWGO sensitivity, we have computed the ALP models for few sources in the parameter space m$_a$ = 1neV - 1μeV and $g_{a\gamma} = 1\times10^{-11} - 1\times10^{-10}$ GeV^{-1}. This region is highlighted in Fig. 3.8.

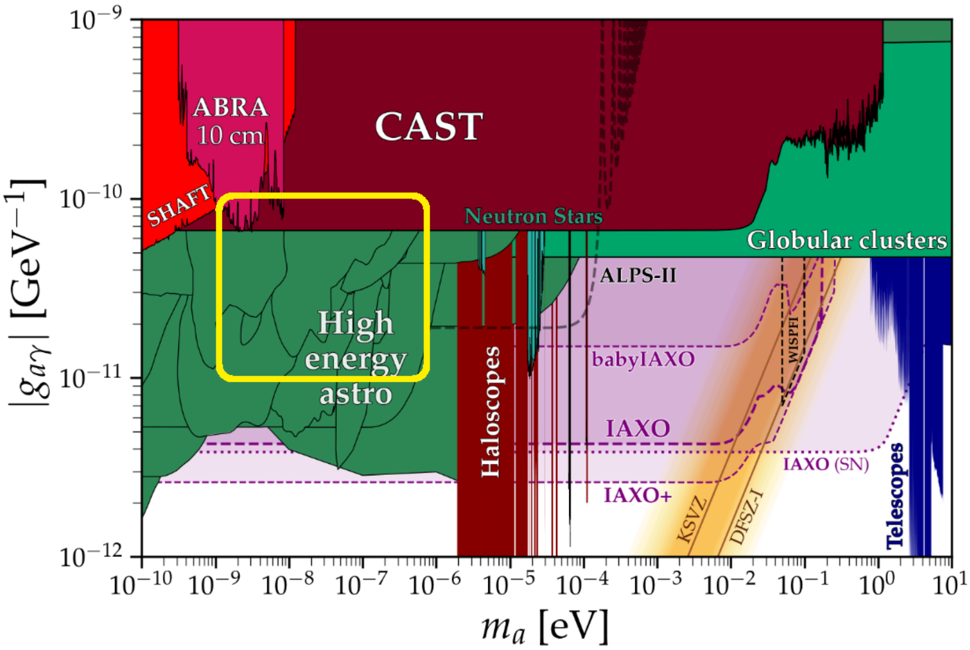

Figure 3.8: Closeup of high energy astrophysical constraints in ALP parameter space. `https://cajohare.github.io/AxionLimits/`

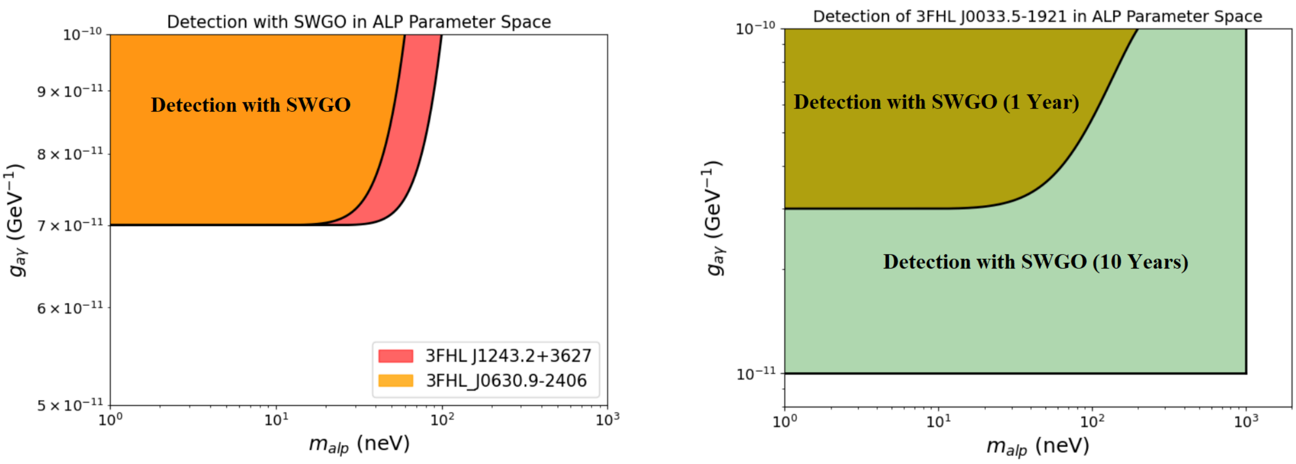

(a) (b)

Figure 3.9: ALP parameter space for the detection of the sources with SWGO

In this way we can also test the sensitivity of SWGO anticipating the detection of sources with SWGO in the future. For instance Fig. 3.9(a) shows the detection of the sources 3FHL J0630.9-2406 and 3FHL J1243.2+3627 with ten years SWGO sensitivity in the considered ALP parameter space. It can be seen that these sources are the most distant ones in our analysis and therefore, they are only detected within the limits highlighted in Fig. 3.9(a). We can conclude that the SWGO data of very distant sources satisfying the same physical conditions used in this analysis, cannot be used to exclude the ALP parameters outside the colored region in the above plot. Furthermore, Fig.3.9(b) shows the detection of 3FHL J0033.5-1921 with one year and ten years SWGO sensitivity. It is evident that SWGO can get the detection for this source in the complete ALP parameter space with ten years sensitivity. While with one year sensitivity, SWGO can only get the detection above $g_{a\gamma} \geq 3 \times 10^{-11}$ GeV^{-1} in colored region establishing a constraint on using the SWGO data for this source to exclude the ALP models in future. The same simulation was done for the rest of the blazar sources to study their detection prospects in the ALP parameter space. They were found to be detected in the considered ALP parameter space, providing us an opportunity to use their SWGO data to derive constraints on the ALP parameters in future. Fig. 3.10 shows the highlighted region between m$_a$ = 1neV - 1μeV and $g_{a\gamma} = 1 \times 10^{-11} - 1 \times 10^{-10}$ GeV^{-1} for the sources detected with SWGO in the considered ALP parameter space.

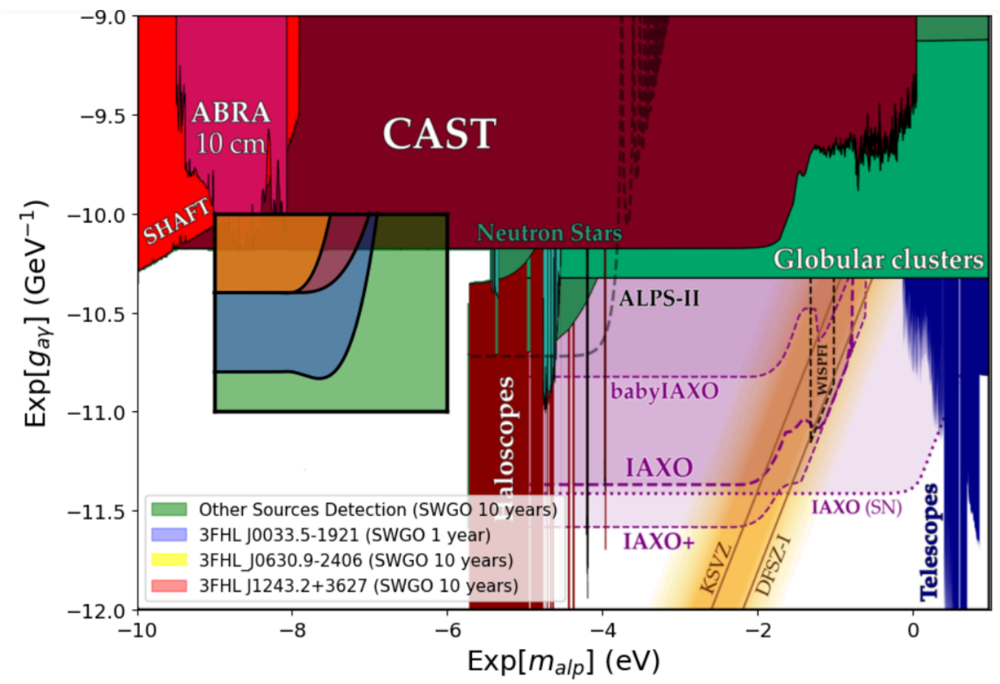

Figure 3.10: Closeup of high energy astrophysical constraints in ALP parameter showing SWGO detectability between m$_a$ = 1neV - 1μeV and $g_{a\gamma} = 1 \times 10^{-11} - 1 \times 10^{-10}$ GeV^{-1} computed in this study.

Chapter 4
Conclusions and Future Work

To conclude, the thesis started by offering insights on axions and PQ formalism [1] in which axions are introduced as a potential Dark Matter candidate in Physics beyond the Standard Model. The same study [1] proposed axions as the possible solution for CP violation in strong interactions. Axions can be extended to a broader category of particles known as ALPs. This thesis focuses on a certain kind of interaction in which ALPs are converted into photons in the presence of external electric or magnetic fields [6]. This phenomenon can be used to search for ALPs indirectly while investigating the VHE gamma rays emitted from extragalactic sources such as AGNs. This relates to one of the aims of this thesis which is to look for ALP signatures in the VHE gamma ray spectrum of extragalactic sources. Moreover, in chapter 1, we have discussed in detail the theoretical background of ALP-photon mixing, consequently presenting the mathematical formula for ALP-photon conversion probability. We discussed the nature and impact of magnetic fields that are involved in the ALP-photon mixing and their propagation from an extragalactic source to the Milky Way. This includes the jet magnetic field, intracluster magnetic field, intergalactic magnetic field, and the Milky Way galactic magnetic field. Since the main aim of this thesis is to test the sensitivity of the next generation gamma-ray detector SWGO, therefore, the thesis also offered some insights into the state of the art searches for ALPs with current gamma-ray detectors on Earth including IACTs and ground-level particle detectors such as HAWC and LHAASO.

We have done a detailed analysis to investigate the affect of ALPs on the spectra of blazar sources and anticipate if the sources are detectable by SWGO or not. We have performed our analysis on twelve blazar sources (BL Lacs) selected from 3FHL Fermi catalog. These sources are the hardest and the most intense sources with known redshift available in the catalog. In order to apply the ALP analysis on the data, first, we have modelled the multiwavelength spectra of the sources using MMDC. Chapter 2 explains the complete methodology of the analysis, starting from accessing the multiwavelength data of the sources until computing the spectra with ALP models. The main task before modelling of the spectrum is to clean the data. It is required because the multiwavelength data is highly variable and contains outliers that can disrupt the modelling. As a final step, we have computed the ALP-photon mixing probability for a few ALP models using `GammaALPs` and then applied it on the intrinsic spectra of the sources to look for a change in the spectra due to ALPs. We computed the ALP models in the parameter space where m_a = 1 neV - 1 μeV and $g_{a\gamma} = 1 \times 10^{-11} - 1 \times 10^{-10}$ GeV^{-1}. Complete results after the analysis are discussed in chapter 3. We can conclude that, among the twelve sources, only two sources 3FHL J0630.9-2406 (z = 1.238) and 3FHL J1243.2+3627 (z = 1.065) can be detected by SWGO only if ALPs existed, satisfying the conditions of mass and coupling required for making the spectra sensitive to SWGO. Eight sources

3FHL J0449.4-4350 (z = 0.205), 3FHL J1217.9+3006 (z = 0.130), 3FHL J1959.9+6508 (z = 0.047), 3FHL J2158.8-3013 (z = 0.116), 3FHL J0809.8+5218 (z = 0.138), 3FHL J1015.0+4926 (z = 0.212), 3FHL J0650.7+2503 (z = 0.203), 3FHL J0033.5-1921 (z = 0.610) can be detected by SWGO in both cases; if ALPs existed and even if ALPs do not exist as the observed spectra still lies above the SWGO sensitivity. The rest of the sources, 3FHL J0738.1+1742 (z = 0.424) and 3FHL J1230.2+2517 (0.135) are not detected by SWGO even if the ALP-photon mixing occurs and alters the spectra. Consequently, these two sources cannot be used to exclude the ALP models as their spectra is below SWGO sensitivity. Although these two sources are not very far but they both have high power-law index (above 2.5) and therefore their spectra become softer around 100 GeV. Table 4.1 summarizes the detection results for all the sources. In the results section, we also discussed the detection of a few sources with SWGO in the ALP parameter space and derived constraints on the detectablity of the sources highlighting the parameter space that can be used to exclude ALP models in future.

Source	Detection with ALPs	Detection without ALPs
3FHL J0449.4-4350	Yes	Yes
3FHL J0630.9-2406	Yes	No
3FHL J0738.1+1742	No	No
3FHL J1217.9+3006	Yes	Yes
3FHL J1230.2+2517	No	No
3FHL J1959.9+6508	Yes	Yes
3FHL J2158.8-3013	Yes	Yes
3FHL J0809.8+5218	Yes	Yes
3FHL J1015.0+4926	Yes	Yes
3FHL J0650.7+2503	Yes	Yes
3FHL J0033.5-1921	Yes	Yes
3FHL J1243.2+3627	Yes	No

Table 4.1: Detection of the sources with and without ALPs

In the analysis, we have used the weighted average technique on multiwavelength data to remove the flux data with multiple frequency (energy) points. This technique is not very reliable for the sources which contain variable states of the flux. In order to deal with this issue, adaptive binning can be a solution. Due to time constraints and considering the scope of this project, we were not able to explore and apply the adaptive binning technique on our data leaving this as an opportunity for the future studies. Secondly, while doing the ALP analysis, we discussed in chapter 2 that we assumed the magnetic field of the jet for all the sources with helical and tangled component. Moreover, we used the jet parameters of Mkn 501 for all our sources while computing the ALP-photon propagation using `GammaALPs`. In this regard, may be in future, this study can be extended in which ALP-photon propagation can be computed with different kind of astrophysical environments involving different jet magnetic field or may be assuming different model for the Milky Way. Also, in future article, we can use the fitting jet parameters for the sources that we are working with if they are investigated or become available in some future study.

References

[1] R. D. Peccei and H. R. Quinn, "CP Conservation in the presence of pseudoparticles," *Phys. Rev. Lett.*, vol. 38, pp. 1440–1443, 25 Jun. 1977. DOI: 10.1103/PhysRevLett.38.1440. [Online]. Available: https://link.aps.org/doi/10.1103/PhysRevLett.38.1440.

[2] S. Jacobsen, T. Linden, and K. Freese, "Constraining axion-like particles with hawc observations of tev blazars," 2022. arXiv: 2203.04332 [hep-ph].

[3] A. De Angelis, O. Mansutti, and M. Roncadelli, "Axion-like particles, cosmic magnetic fields and gamma-ray astrophysics," *Physics Letters B*, vol. 659, pp. 847–855, Feb. 2008. DOI: 10.1016/j.physletb.2007.12.012.

[4] S. Weinberg, "A new light boson?" *Phys. Rev. Lett.*, vol. 40, pp. 223–226, 4 Jan. 1978. DOI: 10.1103/PhysRevLett.40.223. [Online]. Available: https://link.aps.org/doi/10.1103/PhysRevLett.40.223.

[5] F. Wilczek, "Problem of strong P and T invariance in the presence of instantons," *Phys. Rev. Lett.*, vol. 40, pp. 279–282, 5 Jan. 1978. DOI: 10.1103/PhysRevLett.40.279. [Online]. Available: https://link.aps.org/doi/10.1103/PhysRevLett.40.279.

[6] D. A. Dicus, E. W. Kolb, V. L. Teplitz, and R. V. Wagoner, "Astrophysical bounds on the masses of axions and higgs particles," *Phys. Rev. D*, vol. 18, pp. 1829–1834, 6 Sep. 1978. DOI: 10.1103/PhysRevD.18.1829. [Online]. Available: https://link.aps.org/doi/10.1103/PhysRevD.18.1829.

[7] G. Raffelt and L. Stodolsky, "Mixing of the photon with low-mass particles," *Phys. Rev. D*, vol. 37, pp. 1237–1249, 5 Mar. 1988. DOI: 10.1103/PhysRevD.37.1237. [Online]. Available: https://link.aps.org/doi/10.1103/PhysRevD.37.1237.

[8] A. De Angelis, G. Galanti, and M. Roncadelli, "Relevance of axionlike particles for very-high-energy astrophysics," *Phys. Rev. D*, vol. 84, p. 105 030, 10 Nov. 2011. DOI: 10.1103/PhysRevD.84.105030. [Online]. Available: https://link.aps.org/doi/10.1103/PhysRevD.84.105030.

[9] D. Horns, L. Maccione, M. Meyer, A. Mirizzi, D. Montanino, and M. Roncadelli, "Hardening of tev gamma spectrum of active galactic nuclei in galaxy clusters by conversions of photons into axionlike particles," *Phys. Rev. D*, vol. 86, p. 075 024, 7 Oct. 2012. DOI: 10.1103/PhysRevD.86.075024. [Online]. Available: https://link.aps.org/doi/10.1103/PhysRevD.86.075024.

[10] Q. Yu and D. Horns, "Searching for photon-alps mixing effects in agn gamma-ray energy spectra," *Journal of Cosmology and Astroparticle Physics*, vol. 2023, no. 05, p. 029, May 2023, ISSN: 1475-7516. DOI: 10.1088/1475-7516/2023/05/029. [Online]. Available: http://dx.doi.org/10.1088/1475-7516/2023/05/029.

[11] M. Meyer, D. Montanino, and J. Conrad, "On detecting oscillations of gamma rays into axion-like particles in turbulent and coherent magnetic fields," *Journal of Cosmology and Astroparticle Physics*, vol. 2014, no. 09, 003–003, Jan. 2017, ISSN: 1475-7516. DOI: 10.1088/1475-7516/2014/09/003. [Online]. Available: http://dx.doi.org/10.1088/1475-7516/2014/09/003.

[12] I. Batković, A. Angelis, M. Doro, and M. Manganaro, "Axion-like particle searches with iacts," Jun. 2021. DOI: 10.3390/universe7060185. [Online]. Available: http://dx.doi.org/10.3390/universe7060185.

[13] A. De Angelis and M. Pimenta, *Introduction to Particle and Astroparticle Physics: Multimessenger Astronomy and its Particle Physics Foundations* (Undergraduate Lecture Notes in Physics). Heidelberg: Springer Nature, 2018, ISBN: 978-3-319-78180-8, 978-3-319-78181-5.

[14] G. Long, S. Chen, S. Xu, and H.-H. Zhang, "Probing μeV alps with future lhaaso observations of agn γ-ray spectra," *Phys. Rev. D*, vol. 104, p. 083 014, 8 2021. DOI: 10.1103/PhysRevD.104.083014. [Online]. Available: https://link.aps.org/doi/10.1103/PhysRevD.104.083014.

[15] R. E. Pudritz, M. J. Hardcastle, and D. C. Gabuzda, "Magnetic fields in astrophysical jets: From launch to termination," *Space Science Reviews*, vol. 169, no. 1–4, 27–72, Jun. 2012, ISSN: 1572-9672. DOI: 10.1007/s11214-012-9895-z. [Online]. Available: http://dx.doi.org/10.1007/s11214-012-9895-z.

[16] S. O'Sullivan and D. Gabuzda, "Magnetic field strength and spectral distribution of six parsec-scale active galactic nuclei jets," *Monthly Notices of the Royal Astronomical Society*, vol. 400, pp. 26 –42, Nov. 2009. DOI: 10.1111/j.1365-2966.2009.15428.x.

[17] A. Celotti and G. Ghisellini, "The power of blazar jets," *Mon. Not. Roy. Astron. Soc.*, vol. 385, p. 283, 2008. DOI: 10.1111/j.1365-2966.2007.12758.x. arXiv: 0711.4112 [astro-ph].

[18] F. Tavecchio, G. Ghisellini, G. Ghirlanda, L. Foschini, and L. Maraschi, "TeV BL Lac objects at the dawn of the Fermi era," *Mon. Not. Roy. Astron. Soc.*, vol. 401, p. 1570, 2010. DOI: 10.1111/j.1365-2966.2009.15784.x. arXiv: 0909.0651 [astro-ph.HE].

[19] R. Blandford and A. Konigl, "Relativistic jets as compact radio sources.," *Astrophysical Journal*, vol. 232, pp. 34–48, Aug. 1979. DOI: 10.1086/157262.

[20] M. C. Begelman, R. D. Blandford, and M. J. Rees, "Theory of extragalactic radio sources," *Rev. Mod. Phys.*, vol. 56, pp. 255–351, 2 1984. DOI: 10.1103/RevModPhys.56.255. [Online]. Available: https://link.aps.org/doi/10.1103/RevModPhys.56.255.

[21] M. J. Rees, "Magnetic confinement of broad-line clouds in active galactic nuclei," *Monthly Notices of the Royal Astronomical Society*, vol. 228, pp. 47–50, 1 Sep. 1987. [Online]. Available: https://doi.org/10.1093/mnras/228.1.47P.

[22] F. Govoni and L. Feretti, "Magnetic fields in clusters of galaxies," *International Journal of Modern Physics D*, vol. 13, no. 08, 1549–1594, Sep. 2004, ISSN: 1793-6594. DOI: 10.1142/s0218271804005080. [Online]. Available: http://dx.doi.org/10.1142/S0218271804005080.

[23] L. Feretti, G. Giovannini, F. Govoni, and et al, "Clusters of galaxies: Observational properties of the diffuse radio emission," *Astron Astrophys Rev*, vol. 20, p. 54, May 2012. [Online]. Available: https://doi.org/10.1007/s00159-012-0054-z.

[24] K. N. Gourgouliatos, J. Braithwaite, and M. Lyutikov, "Structure of magnetic fields in intracluster cavities: Magnetic fields in intracluster cavities," *Monthly Notices of the Royal Astronomical Society*, vol. 409, no. 4, 1660–1668, Oct. 2010, ISSN: 0035-8711. DOI: 10.1111/j.1365-2966.2010.17410.x. [Online]. Available: http://dx.doi.org/10.1111/j.1365-2966.2010.17410.x.

[25] M. Ackermann and et al, "The search for spatial extension in high-latitude sources detected by the fermi large area telescope," *The Astrophysical Journal Supplement Series*, vol. 237, no. 2, p. 32, Aug. 2018, ISSN: 1538-4365. DOI: 10.3847/1538-4365/aacdf7. [Online]. Available: http://dx.doi.org/10.3847/1538-4365/aacdf7.

[26] G. Sigl, F. Miniati, and T. A. Enßlin, "Ultrahigh energy cosmic ray probes of large scale structure and magnetic fields," *Physical Review D*, vol. 70, no. 4, Aug. 2004, ISSN: 1550-2368. DOI: 10.1103/physrevd.70.043007. [Online]. Available: http://dx.doi.org/10.1103/PhysRevD.70.043007.

[27] K. Dolag, D. Grasso, V. Springel, and I. Tkachev, "Constrained simulations of the magnetic field in the local universe and the propagation of ultrahigh energy cosmic rays," *Journal of Cosmology and Astroparticle Physics*, vol. 2005, no. 01, 009–009, Jan. 2005, ISSN: 1475-7516. DOI: 10.1088/1475-7516/2005/01/009. [Online]. Available: http://dx.doi.org/10.1088/1475-7516/2005/01/009.

[28] A Domínguez, M. Sánchez-Conde, and F Prada, "Axion-like particle imprint in cosmological very-high-energy sources," *Journal of Cosmology and Astroparticle Physics*, vol. 2011, no. 11, 020–020, Nov. 2011, ISSN: 1475-7516. DOI: 10.1088/1475-7516/2011/11/020. [Online]. Available: http://dx.doi.org/10.1088/1475-7516/2011/11/020.

[29] M. Simet, D. Hooper, and P. D. Serpico, "Milky way as a kiloparsec-scale axionscope," *Physical Review D*, vol. 77, no. 6, Mar. 2008, ISSN: 1550-2368. DOI: 10.1103/physrevd.77.063001. [Online]. Available: http://dx.doi.org/10.1103/PhysRevD.77.063001.

[30] R. Jansson and G. R. Farrar, "A new model of the galactic magnetic field," *The Astrophysical Journal*, vol. 757, no. 1, p. 14, Aug. 2012, ISSN: 1538-4357. DOI: 10.1088/0004-637x/757/1/14. [Online]. Available: http://dx.doi.org/10.1088/0004-637X/757/1/14.

[31] M. Meyer, J. Davies, and J. Kuhlmann, "Gammaalps: An open-source python package for computing photon-axion-like-particle oscillations in astrophysical environments," in *Proceedings of 37th International Cosmic Ray Conference — PoS(ICRC2021)*,

ser. ICRC2021, Sissa Medialab, Jun. 2021. DOI: 10.22323/1.395.0557. [Online]. Available: http://dx.doi.org/10.22323/1.395.0557.

[32] M. Spurio, *Probes of Multimessenger Astrophysics: Charged cosmic rays, neutrinos, γ-rays and gravitational waves* (Astronomy and Astrophysics Library). Springer, 2018. DOI: 10.1007/978-3-319-96854-4.

[33] J. D. Finke, S. Razzaque, and C. D. Dermer, "Modeling the extragalactic background light from stars and dust," *The Astrophysical Journal*, vol. 712, no. 1, 238–249, Feb. 2010, ISSN: 1538-4357. DOI: 10.1088/0004-637x/712/1/238. [Online]. Available: http://dx.doi.org/10.1088/0004-637X/712/1/238.

[34] E. Dwek and F. Krennrich, "The extragalactic background light and the gamma-ray opacity of the universe," *Astroparticle Physics*, vol. 43, 112–133, Mar. 2013, ISSN: 0927-6505. DOI: 10.1016/j.astropartphys.2012.09.003. [Online]. Available: http://dx.doi.org/10.1016/j.astropartphys.2012.09.003.

[35] A. Domínguez and et al, "Extragalactic background light inferred from aegis galaxy-sed-type fractions: Ebl from aegis galaxy-sed-type fractions," *Monthly Notices of the Royal Astronomical Society*, vol. 410, no. 4, 2556–2578, Oct. 2010, ISSN: 0035-8711. DOI: 10.1111/j.1365-2966.2010.17631.x. [Online]. Available: http://dx.doi.org/10.1111/j.1365-2966.2010.17631.x.

[36] A. Franceschini, G. Rodighiero, and M. Vaccari, "Extragalactic optical-infrared background radiation, its time evolution and the cosmic photon-photon opacity," vol. 487, no. 3, pp. 837–852, Sep. 2008. DOI: 10.1051/0004-6361:200809691. arXiv: 0805.1841 [astro-ph].

[37] R. C. Gilmore, R. S. Somerville, J. R. Primack, and A. Domínguez, "Semi-analytic modelling of the extragalactic background light and consequences for extragalactic gamma-ray spectra: Modelling of the ebl and gamma-ray spectra," *Monthly Notices of the Royal Astronomical Society*, vol. 422, no. 4, 3189–3207, Apr. 2012, ISSN: 0035-8711. DOI: 10.1111/j.1365-2966.2012.20841.x. [Online]. Available: http://dx.doi.org/10.1111/j.1365-2966.2012.20841.x.

[38] N. Magnussen, "The magic telescope project for gamma astronomy above 10 gev," 1998. arXiv: astro-ph/9805184.

[39] T. Weekes and et al, "Veritas: The very energetic radiation imaging telescope array system," *Astroparticle Physics*, vol. 17, no. 2, 221–243, May 2002, ISSN: 0927-6505. DOI: 10.1016/s0927-6505(01)00152-9. [Online]. Available: http://dx.doi.org/10.1016/S0927-6505(01)00152-9.

[40] J. Hinton, "The status of the hess project," *New Astronomy Reviews*, vol. 48, no. 5–6, 331–337, Apr. 2004, ISSN: 1387-6473. DOI: 10.1016/j.newar.2003.12.004. [Online]. Available: http://dx.doi.org/10.1016/j.newar.2003.12.004.

[41] G. SINNIS, A. SMITH, and J. E. MCENERY, "Hawc: A next generation all-sky vhe gamma-ray telescope," in *The Tenth Marcel Grossmann Meeting*, World Scientific Publishing

Company, Feb. 2006. DOI: 10.1142/9789812704030_0066. [Online]. Available: http://dx.doi.org/10.1142/9789812704030_0066.

[42] Z. Cao and et al, "The large high altitude air shower observatory (lhaaso) science book (2021 edition)," 2022. arXiv: 1905.02773.

[43] J. Hinton, "The southern wide-field gamma-ray observatory: Status and prospects," 2021. arXiv: 2111.13158 [astro-ph.IM].

[44] G. D. Sciascio, "Ground-based gamma-ray astronomy: An introduction," *Journal of Physics: Conference Series*, vol. 1263, no. 1, p. 012 003, Jun. 2019, ISSN: 1742-6596. DOI: 10.1088/1742-6596/1263/1/012003. [Online]. Available: http://dx.doi.org/10.1088/1742-6596/1263/1/012003.

[45] A. Abeysekara and et al, "On the sensitivity of the hawc observatory to gamma-ray bursts," *Astroparticle Physics*, vol. 35, no. 10, 641–650, May 2012, ISSN: 0927-6505. DOI: 10.1016/j.astropartphys.2012.02.001. [Online]. Available: http://dx.doi.org/10.1016/j.astropartphys.2012.02.001.

[46] Z. Cao and et al, "Ultrahigh-energy photons up to 1.4 petaelectronvolts from 12 gamma-ray galactic sources," *nat*, vol. 594, no. 7861, pp. 33–36, Jun. 2021. DOI: 10.1038/s41586-021-03498-z.

[47] U. Barres de Almeida, "The Southern Wide Field Gamma-Ray Observatory (SWGO)," in *43rd COSPAR Scientific Assembly. Held 28 January - 4 February*, vol. 43, Jan. 2021, 1295, p. 1295.

[48] "New cast limit on the axion–photon interaction," *Nature Physics*, vol. 13, no. 6, 584–590, May 2017, ISSN: 1745-2481. DOI: 10.1038/nphys4109. [Online]. Available: http://dx.doi.org/10.1038/nphys4109.

[49] J. Vogel *et al.*, "The next generation of axion helioscopes: The international axion observatory (iaxo)," English, *Physics Procedia*, vol. 61, pp. 193–200, 2015, This is an open access article under the CC BY-NC-ND license (http://creativecommons.org/licenses/by-nc-nd/3.0/)., ISSN: 1875-3892. DOI: 10.1016/j.phpro.2014.12.031.

[50] R. Ballou *et al.*, "New exclusion limits on scalar and pseudoscalar axionlike particles from light shining through a wall," *Physical Review D*, vol. 92, no. 9, Nov. 2015, ISSN: 1550-2368. DOI: 10.1103/physrevd.92.092002. [Online]. Available: http://dx.doi.org/10.1103/PhysRevD.92.092002.

[51] R. Barbieri *et al.*, "Searching for galactic axions through magnetized media: The quax proposal," *Physics of the Dark Universe*, vol. 15, 135–141, Mar. 2017, ISSN: 2212-6864. DOI: 10.1016/j.dark.2017.01.003. [Online]. Available: http://dx.doi.org/10.1016/j.dark.2017.01.003.

[52] N. Du and et al, "Search for invisible axion dark matter with the axion dark matter experiment," *Physical Review Letters*, vol. 120, no. 15, Apr. 2018, ISSN: 1079-7114. DOI: 10.1103/physrevlett.120.151301. [Online]. Available: http://dx.doi.org/10.1103/PhysRevLett.120.151301.

[53] F. Aharonian and et al, "A low level of extragalactic background light as revealed by gamma-rays from blazars," *Nature*, vol. 440, no. 7087, 1018–1021, Apr. 2006, ISSN: 1476-4687. DOI: 10.1038/nature04680. [Online]. Available: http://dx.doi.org/10.1038/nature04680.

[54] D. Mazin and M. Raue, "New limits on the density of the extragalactic background light in the optical to the far-infrared from the spectra of all known TeV blazars," *Astron. Astrophys.*, vol. 471, pp. 439–452, 2007. DOI: 10.1051/0004-6361:20077158. arXiv: astro-ph/0701694.

[55] D. Hooper and P. D. Serpico, "Detecting axionlike particles with gamma ray telescopes," *Phys. Rev. Lett.*, vol. 99, p. 231 102, 23 2007. DOI: 10.1103/PhysRevLett.99.231102. [Online]. Available: https://link.aps.org/doi/10.1103/PhysRevLett.99.231102.

[56] A. De Angelis, M. Roncadelli, and O. Mansutti, "Evidence for a new light spin-zero boson from cosmological gamma-ray propagation?" *Physical Review D*, vol. 76, Aug. 2007. DOI: 10.1103/PHYSREVD.76.121301.

[57] M. A. Sánchez-Conde, D. Paneque, E. Bloom, F. Prada, and A. Domínguez, "Hints of the existence of axionlike particles from the gamma-ray spectra of cosmological sources," *Physical Review D*, vol. 79, no. 12, Jun. 2009, ISSN: 1550-2368. DOI: 10.1103/physrevd.79.123511. [Online]. Available: http://dx.doi.org/10.1103/PhysRevD.79.123511.

[58] A. Mirizzi and D. Montanino, "Stochastic conversions of tev photons into axion-like particles in extragalactic magnetic fields," *Journal of Cosmology and Astroparticle Physics*, vol. 2009, no. 12, 004–004, Jan. 2017, ISSN: 1475-7516. DOI: 10.1088/1475-7516/2009/12/004. [Online]. Available: http://dx.doi.org/10.1088/1475-7516/2009/12/004.

[59] A. Abramowski and et al, "Constraints on axionlike particles with h.e.s.s. from the irregularity of the pks 2155-304 energy spectrum," *Physical Review D*, vol. 88, no. 10, Nov. 2013, ISSN: 1550-2368. DOI: 10.1103/physrevd.88.102003. [Online]. Available: http://dx.doi.org/10.1103/PhysRevD.88.102003.

[60] H. Abe and et al, "Constraints on axion-like particles with the perseus galaxy cluster with magic," *Physics of the Dark Universe*, vol. 44, p. 101 425, May 2024, ISSN: 2212-6864. DOI: 10.1016/j.dark.2024.101425. [Online]. Available: http://dx.doi.org/10.1016/j.dark.2024.101425.

[61] L. Mastrototaro *et al.*, "Constraining axion-like particles with the diffuse gamma-ray flux measured by the large high altitude air shower observatory," *The European Physical Journal C*, vol. 82, no. 11, Nov. 2022, ISSN: 1434-6052. DOI: 10.1140/epjc/s10052-022-10979-6. [Online]. Available: http://dx.doi.org/10.1140/epjc/s10052-022-10979-6.

[62] J. Li, X.-J. Bi, L.-Q. Gao, X. Huang, R.-M. Yao, and P.-F. Yin, "Constraints on axion-like particles from the observation of galactic sources by lhaaso," 2024. arXiv: 2401.01829 [astro-ph.HE].

[63] X. Bi *et al.*, “Axion and dark photon limits from crab nebula high-energy gamma rays,” *Phys. Rev. D*, vol. 103, p. 043 018, 4 2021. DOI: 10.1103/PhysRevD.103.043018. [Online]. Available: https://link.aps.org/doi/10.1103/PhysRevD.103.043018.

[64] R. Conceição, *The southern wide-field gamma-ray observatory*, 2023. arXiv: 2309.04577 [hep-ex].

[65] M. Ajello and et al, “3fhl: The third catalog of hard fermi-lat sources,” *The Astrophysical Journal Supplement Series*, vol. 232, no. 2, p. 18, Sep. 2017, ISSN: 1538-4365. DOI: 10.3847/1538-4365/aa8221. [Online]. Available: http://dx.doi.org/10.3847/1538-4365/aa8221.

[66] W. B. Atwood and et al, “The large area telescope on thefermi gamma-ray space telescopemission,” *The Astrophysical Journal*, vol. 697, no. 2, 1071–1102, May 2009, ISSN: 1538-4357. DOI: 10.1088/0004-637x/697/2/1071. [Online]. Available: http://dx.doi.org/10.1088/0004-637X/697/2/1071.

[67] D. J. Thompson and C. A. Wilson-Hodge, “Fermi gamma-ray space telescope,” in *Handbook of X-ray and Gamma-ray Astrophysics*. Springer Nature Singapore, Nov. 2022, 1–31, ISBN: 9789811645440. DOI: 10.1007/978-981-16-4544-0_58-1. [Online]. Available: http://dx.doi.org/10.1007/978-981-16-4544-0_58-1.

[68] S. Abdollahi and et al, “Fermi large area telescope fourth source catalog,” *The Astrophysical Journal Supplement Series*, vol. 247, no. 1, p. 33, Mar. 2020, ISSN: 1538-4365. DOI: 10.3847/1538-4365/ab6bcb. [Online]. Available: http://dx.doi.org/10.3847/1538-4365/ab6bcb.

[69] G. Principe, “The fermi gamma ray sky: Summary of recent observations,” 2022. arXiv: 2209.03652 [astro-ph.HE]. [Online]. Available: https://arxiv.org/abs/2209.03652.

[70] S. Abdollahi and et al, “Incremental fermi large area telescope fourth source catalog,” *The Astrophysical Journal Supplement Series*, vol. 260, no. 2, p. 53, Jun. 2022, ISSN: 1538-4365. DOI: 10.3847/1538-4365/ac6751. [Online]. Available: http://dx.doi.org/10.3847/1538-4365/ac6751.

[71] C. Deil and et al, “Gammapy - a prototype for the cta science tools,” 2017. arXiv: 1709.01751 [astro-ph.IM]. [Online]. Available: https://arxiv.org/abs/1709.01751.

[72] D. Tripathi and et al, “Firmamento: A multi-messenger astronomy tool for citizen and professional scientists,” 2024. arXiv: 2311.15102 [astro-ph.HE]. [Online]. Available: https://arxiv.org/abs/2311.15102.

[73] D. Bégué *et al.*, “Modeling blazar broadband emission with convolutional neural networks – i. synchrotron self-compton model,” 2023. arXiv: 2311.02979 [astro-ph.HE]. [Online]. Available: https://arxiv.org/abs/2311.02979.

[74] P. Peñil *et al.*, “Multiwavelength variability analysis of fermi-lat blazars,” 2024. arXiv: 2403.01520 [astro-ph.HE]. [Online]. Available: https://arxiv.org/abs/2403.01520.

[75] K. K. Singh, B Bisschoff, B van Soelen, A Tolamatti, J. P. Marais, and P. J. Meintjes, “Long-term multiwavelength view of the blazar 1es 1218+304,” *Monthly Notices of the Royal Astronomical Society*, vol. 489, no. 4, 5076–5086, Sep. 2019, ISSN: 1365-2966. DOI: 10.1093/mnras/stz2521. [Online]. Available: http://dx.doi.org/10.1093/mnras/stz2521.

[76] C. Nigro, J. Sitarek, P. Gliwny, D. Sanchez, A. Tramacere, and M. Craig, “Agnpy: An open-source python package modelling the radiative processes of jetted active galactic nuclei,” *Astronomy amp; Astrophysics*, vol. 660, A18, Apr. 2022, ISSN: 1432-0746. DOI: 10.1051/0004-6361/202142000. [Online]. Available: http://dx.doi.org/10.1051/0004-6361/202142000.

[77] W. J. Potter and G. Cotter, “New constraints on the structure and dynamics of black hole jets,” *Monthly Notices of the Royal Astronomical Society*, vol. 453, no. 4, 4071–4089, Sep. 2015, ISSN: 1365-2966. DOI: 10.1093/mnras/stv1657. [Online]. Available: http://dx.doi.org/10.1093/mnras/stv1657.

Acronyms

ADMX Axion Dark Matter Experiment.

AGN Active Galactic Nucleus.

ALP Axion-Like Particle.

BLL BL Lacertae.

BPL Broken Power Law.

BSM Beyond the Standard Model.

CAST CERN Axion Solar Telescope.

CMB Cosmic Microwave Background.

CTA Cherenkov Telescope Array.

DM Dark Matter.

EAS Extensive Air Shower.

EBL Extragalactic Background Light.

EC External Compton.

ECLP Log Parabola with an Exponential Cut-off.

ECPL Power Law with an Exponential Cut-off.

Fermi-LAT Fermi Large Area Telescope.

FoV Field of View.

FSRQ Flat Spectrum Radio Quasars.

H.E.S.S. High Energy Stereoscopic System.

HAWC High Altitude Water Cherenkov.

IACT Imaging Atmospheric Cherenkov Telescope.

IAXO International Axion Observatory.

IGMF Intergalactic Magnetic Field.

LHAASO Large High Altitude Air Shower Observatory.

LOS Line of Sight.

LP Log Parabola.

MAGIC Major Atmospheric Gamma Imaging Cherenkov.

MCMC Markov chain Monte Carlo.

PL Power Law.

QCD Quantum Chromodynamics.

QUAX Quest for Axions.

SED Spectral Energy Distribution.

SSC Synchrotron self-Compton.

SWGO Southern Wide-Field Gamma-ray Observatory.

VERITAS Very Energetic Radiation Imaging Telescope Array System.

VHE Very High Energy.

List of Tables

List of Figures

ACKNOWLEDGEMENTS

I would like to express my deepest gratitude to those who have supported and guided me throughout the journey of completing this thesis. First and foremost, I am immensely grateful to my supervisor, Prof. Michele Doro, for his unwavering support, insightful guidance, and encouragement. Your expertise and commitment to excellence have been invaluable in shaping the direction and quality of my work. I am also thankful to my co-supervisor, Ivana Batkovic, for her constructive feedback and mentorship. You were always ready and available to guide me whenever I got stuck at some point. Your influence has been instrumental in my academic growth. I am very grateful to Paolo Giommi for providing his expertise on the multiwavelength data modelling from the early stages of my work. I am also very thankful to Narek Sahakyan for introducing me to MMDC platform and constantly helping me with any doubts and confusions regarding the blazar modelling.

I would like to extend my heartfelt thanks to my family. To my parents, your love, patience, and belief in my potential have been my constant source of strength. Your sacrifices and encouragement have been the foundation upon which this work is built. To my siblings, thank you for your unwavering support and understanding during the countless hours spent on this thesis. To my cute little nieces, Zubia, Hadiya and Ayesha, thank you for bringing lots of happiness and love in my life during this time. To my friends, Rohan, Ahsan, Ubaid, Muzzammil, Taha, Mahad, Fazl, Umer, Rameez, Fawaz, Tabish, Hassan, Luca, Emerson, Mateen and Eesha, thank you for the laughter, the late-night study sessions, and for always being there when I needed a break or a kind word. Your companionship has made this journey not only bearable but truly enjoyable. Finally, I would like to dedicate this thesis to my aunt (late), your prayers were and are always with me.

At the end, I wish to express my gratitude to everyone else who contributed in any way to the completion of this thesis. Whether through academic collaboration, moral support, or simply by being there when I needed it most, your contributions have not gone unnoticed, and I am deeply appreciative. This thesis is the culmination of the collective efforts and support of all of you, and I am sincerely grateful for everything you have done.